Boltzmann equation studies of off-equilibrium QCD phenomena

Author:
Brandon Viljoen

Supervisor:
Prof. André Peshier

a thesis presented for the degree of

MASTER OF SCIENCE

in the department of Physics

University of Cape Town

February 2016

Declaration of Authorship

I know the meaning of plagiarism and declare that all of the work in this thesis, save for that which is properly acknowledged, is my own.

Signed by candidate

15-02-16

Author Signature

Date

Abstract

Much of the evolution of the quark-gluon plasma (QGP) produced in heavy-ion collisions can be modeled by relativistic (viscous) hydrodynamics, which assumes that the partons are sufficiently close to equilibrium. We would like to explore the dynamics of QGP, even before this (quasi) equilibrium stage is reached. To that end, a useful tool from the stage where we can assume the partons to be on-shell is the relativistic Boltzmann equation. We develop parallel code to solve the relativistic Boltzmann equation in the relaxation time approximation in 3 + 1 dimensions (without simplifying assumptions on possible symmetries of the dynamics). Our approach, solving for the distribution function, will allow us to obtain detailed information about the dynamics of heavy ion collisions beyond hydrodynamics, which specify only bulk properties of the medium. Following recent work, we also explore the possibility of forming a transient Bose-Einstein condensate in a dense system of gluons, such as those found in the early stage of a heavy ion collision. For simplicity, we focus here on purely gluonic systems (without quark degrees of freedom). We first use our code to describe a system undergoing 0 + 1 longitudinal Bjorken expansion, after which we present some first numerical results for a system in the full 3 + 1 dynamics.

Acknowledgments

The financial assistance of the National Research Foundation (NRF) towards this research is hereby acknowledged. Opinions expressed and conclusions arrived at, are those of the author and are not necessarily to be attributed to the NRF.

I would like to thank Prof. André Peshier for his continued patience, guidance and many encouraging comments that have gone a long way to making this MSc possible. Thanks for keeping me interested in physics!

Thanks to Greg Jackson for his helpful comments on this thesis.

Thank you to all of my family for your support and encouragement - especially through the hard times. I would not be where I am without all of you.

Thank you Charlotte for keeping me sane.

Contents

Chapter 1

Introduction

1.1 Heavy Ion Collisions and the QGP

The Relativistic Heavy Ion Collider RHIC and the Large Hadron Collider LHC are modern high-energy particle colliders which have opened up opportunities to probe hadronic matter – matter subject to the strong interaction, which is described by Quantum Chromodynamics (QCD) – under the most extreme conditions. Of particular interest to us are properties of the quark gluon plasma (QGP).

The QGP is a phase of QCD matter formed at sufficiently high temperatures and densities, composed of a dense system of deconfined quarks and gluons. Ordinarily, these partons are confined within the nucleus. At a temperature of $T_c \approx 160$ MeV nuclear matter undergoes a (phase) transition into the QGP state. Experimentally one can probe temperatures above this deconfinement temperature by colliding nuclei at near-to-light speeds. The highly excited system undergoes a complex dynamical evolution [14, 25], which results in the production of a large number of particles, which ultimately stream to the detector. Inferring the properties of the QGP formed in intermediate stages of the collision from the measured observables is the principle goal of the heavy ion programs at the LHC and RHIC. We will now briefly describe this evolution following [14].

Within a single heavy-ion event, incoming nuclei approach each other at almost the speed of light. These nuclei with a Lorentz-factor $\gamma \sim 100$ appear strongly contracted along the beam axis. They are largely composed of gluons (which, however, carry only a small

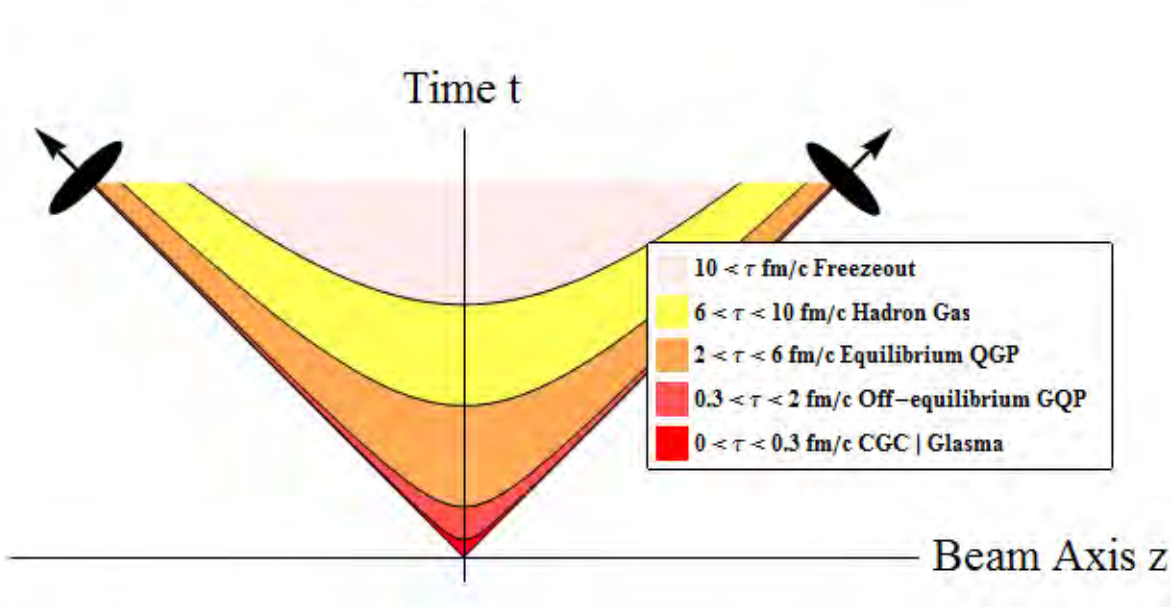

Figure 1.1: Space-time history of the QGP formed in a heavy ion collision at LHC energies. The hyperbolic curves correspond to fixed proper times $\tau = \sqrt{t^2 - z^2/c^2}$. Lorentz contracted nuclei pass through each other at near-to-light speeds, leaving an expanding fireball of QGP matter in their wake. Figure inspired by [23].

fraction of the longitudinal momentum of their nucleons). This state is the so-called coloured glass condensate (CGC). Shortly after collision, a large number of gluons are "liberated" from the CGC. Most of the matter that reaches the detector ultimately stems from hadronization of the gluons produced in this stage. Moments after this liberation, the gluons form a dense, off-equilibrium medium known as the glasma. Hereafter, the partonic matter expands and undergoes a surprisingly rapid thermalization $O(1\text{fm/c})$ which results in a locally equilibrated QGP. In an ultrarelativistic setting characterized by extreme expansion rates, this fast thermalization indicates strong interactions. The medium continues to expand and decrease in density until it drops below the deconfinement temperature T_c, where the partons hadronize (freeze out) and stream to the detector.

Our goal is to shed some light on the dynamics of the QGP from the earliest pre-equilibrium stages, all the way up to thermalization and eventually freeze-out. The framework suitable for the description of off-equilibrium dynamics of the early stages of the collision – shortly after the CGC/Glasma stages – is relativistic kinetic theory [14]: an alternative to (viscous) relativistic hydrodynamics to describe the strong collective behaviour of the QGP.

1.2 Kinetic Theory & Hydrodynamics

The fundamental equation in kinetic theory is the Boltzmann equation. It is a highly nonlinear integro-differential equation that governs the evolution of the distribution function $f(\mathbf{x},\mathbf{p}) = \frac{dN}{d^3x d^3p}$, which represents an average number of particles per phase space volume element. The Boltzmann equation can be stated in a manifestly covariant manner as [8, 25]

$$\underbrace{p^\alpha \partial_\alpha f(\mathbf{x},\mathbf{p})}_{\text{convection}} + \underbrace{mF^\alpha \partial^p_\alpha f(\mathbf{x},\mathbf{p})}_{\text{external force}} = \underbrace{C_{[f(\mathbf{x},\mathbf{p})]}}_{\text{collisions}}. \tag{1.1}$$

The Boltzmann equation is a truncation of the so-called BBGKY (Bogoliov, Born, Green, Kirkwood, Yvon) hierarchy [16, 11], which neglects pair-correlations in N-body interactions. It is suitable for describing the off-equilibrium dynamics of fluids in the "dilute gas regime"[15, 24]. Here, the mean free path λ_{mfp} of the constituent particles is assumed to be much larger than the thermal wavelength λ_{th}, thereby justifying a description in terms of on-shell quasiparticles. The first term in (1.1) is a "convective" derivative ($\frac{1}{p_0}p^\alpha\partial_\alpha = \partial_t + \mathbf{v}\cdot\nabla$) that describes the free propagation of particles at their respective velocities $\mathbf{v}$. The second term accounts for any external forces F^α present. The collision term $C_{[f]}$ describes the interactions (scatterings) between the constituent particles. The Boltzmann equation also obeys the second law of thermodynamics, and conserves energy and momentum and in some cases particle number [8].

The collision term which takes into account quantum effects is due to Uehling and Uhlenbeck [25]

$$C_{[f(\mathbf{x},\mathbf{p})]} = \frac{1}{2}\int \frac{d^3p_*}{E_*}\frac{d^3p'}{E'}\frac{d^3p'_*}{E'_*}\left\{f'f'_*\bar{f}\bar{f}_* W(p',p'_*|p,p_*) - f f_* \bar{f}'\bar{f}'_* W(p,p_*|p',p'_*)\right\} \tag{1.2}$$

where the $\bar{f} = 1 \pm f$ terms represent Bose-enhancement/Pauli-blocking and we have used the shorthand notation

$$f = f(x,p), \qquad f' = f(x,p'), \qquad f_* = f(x,p_*), \qquad f'_* = f(x,p'_*).$$

The transition rate $W(a,b|c,d)$ encodes the probability for a pair of particles with momentum $\{a,b\}$ to produce particles with momentum $\{c,d\}$.

Solving the Boltzmann equation numerically with the collision term (1.2) is challenging, unless certain simplifying assumptions are made on the symmetries of the system. We would like to focus on the full dynamics of the QGP, with no underlying assumptions on the symmetry of the distribution function. This motivates us to employ a phenomenological model for $C_{[f]}$, which hopefully captures essential features of the dynamics.

The relaxation time approximation (RTA), also known as the BGK (Bhatnagar, Gross and Kook)[8] approximation gives an Ansatz for the collision term

$$C^{\mathrm{BGK}}_{[f]} = \frac{f_\infty - f}{\tau_{\mathrm{rel}}}, \tag{1.3}$$

which replaces the complicated form in 1.2 by a single parameter τ_{rel}. This model is motivated by the observation that the main effect of collisions is to drive a system toward a unique equilibrium state f_∞. The relaxation time τ_{rel} controls the speed of the approach of the distribution f to this equilibrium, and is physically related to the typical time between collisions of the interacting particles [8, 13].

Since the flows in heavy ion Physics are ultra-relativistic, we require a fully relativistic scheme. The relaxation time approximation also refers to a model due to Anderson and Witting [2]

$$C^{\mathrm{AW}}_{[f]} = p^\alpha u_\alpha \frac{f_\infty - f}{\tau_{\mathrm{rel}}}, \tag{1.4}$$

which is a manifestly covariant form of the BGK model (1.3). Hereafter, references to the RTA refer to the Anderson and Witting model.

With a choice of the equilibrium distribution f_∞ as the Bose-Einstein (BE), Fermi-Dirac (FD) or Maxwell-Boltzmann (MB) distributions, we can describe both quantum[1] and classical systems [8].

Whilst in principle it would be desirable to describe the full dynamics of the QGP, we here for simplicity consider a system composed entirely of gluons. We do this as a starting

[1] In the dilute gas regime $\lambda_{\mathrm{mfp}} \gg \lambda_{\mathrm{th}}$. For systems where $\lambda_{\mathrm{mfp}} \approx \lambda_{\mathrm{th}}$, the quasiparticle picture begins to break down, and is better described in terms of the Wigner Quasi-probability function, of which the distribution function is formally the $h \to 0$ limit[25].

point for development, but this simplification nonetheless has some physical relevance. The initial state formed shortly after a heavy ion collision is thought to be largely composed of out-of equilibrium gluons, the so-called glasma formed out of the CGC [14]. Whilst we cannot describe the CGC state directly, we can take inspiration from it for our initial conditions. In the context of Boltzmann evolution, it has been argued that the initial gluon densities are parametrically large [5]. As a result, the possibility of forming a transient Bose-Einstein condensate has been recently explored with a QCD Boltzmann equation in the small-angle approximation in a static setting, in a homogeneous volume [7, 6]. The Bose-Einstein condensate is a feature that we can incorporate in our dynamical scheme, which could prove to have a large effect on the dynamics of the QGP. Realistically, these gluons acquire a temperature dependent effective mass due to the nature of the interactions involved [20]. We neglect these effects for the time being and work exclusively with massless gluons.

In contrast to our approach, relativistic hydrodynamics [15, 14, 24] is a course-grained effective theory which describes well the flow of the QGP during intermediate stages of a HIC, when it is close to local equilibrium – See Fig. 1.1. The equations of motion here are "simply" those of energy-momentum conservation $\partial_\alpha T^{\alpha\beta} = 0$ along with any additional conserved currents $\partial_\alpha J^\alpha = 0$. Hydrodynamics describes the evolution of the five fields $\{\mathcal{E}(\mathbf{t},\mathbf{x}), \mathcal{N}(\mathbf{t},\mathbf{x}), \mathbf{u}(\mathbf{t},\mathbf{x})\}$ the energy and particle densities and the relativistic fluid velocity [2]. This evolution depends on information on bulk properties, i.e. the equation of state and so-called transport coefficients.

Underlying these equations is typically an assumption that the distribution function is isotropic in momentum space in its local rest frame. Traditionally, this distribution is taken to be an equilibrium distribution such as the Bose-Einstein or Fermi-Dirac distributions. Together with taking the limit in which interactions within the fluid become infinitely strong ($\tau_{rel} \to 0$ in our relaxation time approximation), we obtain so-called ideal hydrodynamics. This describes a perfect-fluid in which dissipative effects are entirely absent (see section 2.3.2). Viscous hydrodynamics considers deviations from this ideal case

[2] By contrast, the Boltzmann equation evolves the distribution function – a single field over seven variables $f(\mathbf{x}, \mathbf{p}, t)$.

by parametrizing the dissipative (off-equilibrium) effects in terms of so-called transport coefficients such as the shear viscosity η and bulk viscosity Π [15, 24].

In our approach, we have full access to the distribution function $f(\mathbf{x}, \mathbf{p})$, which is free to deviate far from a highly symmetric form such as equilibrium $f_\infty \equiv f_\infty(|\mathbf{p}|)$. Through direct implementation of the Boltzmann equation (1.1) in the relaxation time approximation (1.4), we seek to develop an alternative approach to viscous hydrodynamics, and describe the QGP from before the onset of thermalization all the way up to freeze-out.

In a non-relativistic setting, the equations governing viscous fluids are the familiar Navier-Stokes equations. These equations turn out to be difficult to generalize to a covariant form. Although there are many schemes of viscous relativistic hydrodynamics which have been developed to capture essential features of the underlying microscopic dynamics [12], a fully established relativistic theory is still missing.

In fact, general forms of Hydrodynamics can be derived from the Boltzmann equation in the RTA in a window of weak coupling $\lambda_{mfp}/\lambda_{th} \ll 1$ [15, 24]. Recent exact solutions to the Boltzmann equation in the RTA for the highly symmetric 0+1 dimensional Bjorken flow and 1+1 dimensional conformal Gubser flow have been found, and have been used to test the validity of the various Hydrodynamical schemes [12, 15]. In this spirit, our numerical implementation of the 3+1 dimensional Boltzmann equation could potentially be used to compare various implementations of 3+1 dimensional Hydrodynamics.

1.3 Computational Complexity

The Boltzmann equation (1.1) is a challenging equation to solve numerically. Even in the Relaxation Time Approximation, we still need to evolve the distribution function in time, over a six-dimensional phase space. For illustration, consider that numerically the distribution function must be discretized. It may be represented as a 3+3+1 dimensional (3 spatial, 3 momentum, 1 time) array where each value corresponds to a representative value of the distribution function at a particular point in space, with a particular momen-

tum at a given time. With a relatively course discretization of, say, 100 grid points per dimension, we have 100^6 coupled differential equations to deal with at each time step. To put this into perspective, simply storing such a large system corresponds to ≈ 4 Tera-bytes (4 bytes/float $\times 100^6$ floats $\times 10^{-12}$ Tera-bytes/byte) in a floating-point representation.

It is therefore important to find a suitable means of reducing the complexity of the problem. One obvious way is to consider situations which have a certain symmetry in order to reduce the number of dimensions of the phase space.

A commonly employed simplification in the context of heavy ion physics is the Bjorken picture, in which the expansion of nuclear matter is assumed to be longitudinally boost-invariant [4] – see Section 2.6.1. This simplifies the equations of motion to a form which lets us focus on the distribution at central slice (mid-rapidity) and build up the full solution at any point along the beam axis by longitudinal Lorentz boosts.

Central collisions are highly symmetrical situations which would allow us to assume spatial and momentum isotropy in the transverse directions. Furthermore, as the flow is initially much stronger along the beam axis than in the transverse directions, the transverse expansion could be neglected for a time [24, 25].

However, since we would like to explore the full 3+1 dimensional dynamics, we cannot resort to these simplified symmetries. Another means to reduce the size of the problem is to reduce the number of grid points in the numerical representation of $f(\mathbf{x}, \mathbf{p})$, thereby reducing the number of equations that need solving. The question then becomes: by how much? Is it more important to have fine spatial resolution or momentum resolution?

In a heavy ion collision, the typical size of the system is of the order of the nuclear radius [24]. For instance for an Au-Au collision, we have $R_{Au} \approx 8$ fm. We would like fine spatial resolution to resolve the flow patterns in the expanding matter, but we would also like the spatial cells in our grid to be large enough to contain sufficiently many particles for statistical mechanical concepts to be applicable. In equilibrium at a temperature of approximately twice the confinement temperature $T = 0.4$ GeV, the number of gluons

found in a volume of 1 fm^3 is not large, $N_g \approx (122)T^3 \approx 8$ – see (2.26)). Therefore, using 1 fm^3 as an approximate lower limit for the size of our cell, and the maximum spatial width of our system $L \approx 2R_{Au} \approx 20$ fm suggests that we should expect to implement at most $N_x \approx 20$ grid cells per spatial dimension.

Solving the Boltzmann equation (1.1) involves computing integrals over all momenta [8] – in order to set the equilibrium parameters of the equilibrium function in (1.4) – which will be poorly approximated if we reduce the size of the momentum grid too far. We therefore find it is useful to use Gaussian Quadrature [22] which can provide accurate approximations to these integrals for sufficiently smooth functions, with many fewer points than uniform grid approaches. In our implementation, we have found success with Legendre-Gauss Quadrature, with $N_p = 32$ grid points per momentum dimensions.

1.4 Project Overview

In this project, we develop a full 3+1 dimensional Boltzmann equation solver in the Relaxation Time Approximation for a system of massless gluons. We have done so by reducing the set of equations to a size that fits on a typical modern graphics processing unit (GPU) which is capable of storing approximately 2 Gigabytes. We have greatly reduced the computation time by implementing a parallel algorithm on the GPU using NVidia CUDA [19].

In chapter 2, we present the necessary theory of the Boltzmann equation in the Relaxation Time Approximation, and discuss certain microscopic and macroscopic properties thereof. We also discuss Bose-Einstein condensation, and show some numerical results for its evolution in the Bjorken scenario. In chapter 3, the numerical principles and algorithms used in our implementation are described in some detail. In Chapter 4, some first results of our implementation in 3+1 dimensions are presented, highlighting some of the different features present in a heavy-ion physics context. Finally, we summarize with some comments, conclusions and an outlook for future work. Some useful definitions and details are presented in the Appendices.

Chapter 2

Theory

2.1 Conventions

We set $\hbar = c = k_B = 1$. The choice of Minkowski metric is $g^{\alpha\beta} = \text{diag}(1, -1, -1, -1)$. To simplify our notation we introduce a shorthand for the invariant momentum integration measure

$$\int dP = \frac{g}{(2\pi)^3} \int_{-\infty}^{\infty} \int_{-\infty}^{\infty} \int_{-\infty}^{\infty} dp_x dp_y dp_z \frac{1}{p_0}. \tag{2.1}$$

where g is the degeneracy factor to be defined in the following section and $p_0 = \sqrt{\mathbf{p}^2 + m^2}$. Unless otherwise stated, $\gamma = (1 - \mathbf{u}^2)^{-\frac{1}{2}}$ is always the Lorentz gamma associated with the collective fluid velocity $\mathbf{u}$. In order to lighten the notation whenever the distribution function f appears without arguments it is understood that it is still a function of the position, momentum and time $f \equiv f(\mathbf{x}, \mathbf{p}, t) \equiv \frac{dN}{d^3x d^3p}$.

2.2 One Particle Distribution Function

The four-vectors describing the position and momentum of an on-shell massive relativistic particle are

$$x^\alpha = (t, \mathbf{x}), \tag{2.2}$$

$$p^\alpha = (p_0, \mathbf{p}), \tag{2.3}$$

where the relativistic energy of the particle $p_0 = \sqrt{\mathbf{p}^2 + m^2}$. We note that the lengths of these four-vectors are $x^\alpha x_\alpha = t^2 - \mathbf{x}^2$ and $p^\alpha p_\alpha = m^2$. For the case of massless particles,

the particle energy is simply the magnitude of the particle momentum vector $p_0 = |\mathbf{p}|$ and the momentum is simply the particle wavevector $\mathbf{p} = \mathbf{k}$. This implies that the velocity is the speed of light, $|d\mathbf{x}/dt| = 1$.

The distribution function $f(\mathbf{x}, \mathbf{p})$ is defined as the number of particles located in a volume element d^3x about point $\mathbf{x}$ and with a momentum range of d^3p about momentum $\mathbf{p}$ [25, 8]

$$f(\mathbf{x}, \mathbf{p}) = \frac{dN}{d^3x d^3p}. \tag{2.4}$$

The number of particles dN is independent of the reference frame and is therefore invariant. On the other hand, the volume element transforms under a Lorentz boost with velocity $\mathbf{u}$ as

$$d^3x' = \frac{1}{\gamma} d^3x, \tag{2.5}$$

while in momentum space

$$d^3p' = \gamma d^3p. \tag{2.6}$$

Therefore, we find that the phase space volume element

$$\begin{aligned} d^3x' d^3p' &= \frac{1}{\gamma} d^3x \gamma d^3p \\ &= d^3x d^3p, \end{aligned} \tag{2.7}$$

is a scalar. Consequently the distribution function $f(\mathbf{x}, \mathbf{p})$ itself is also invariant [25].

Additionally, since $p_0' = \gamma p_0$, we have

$$\frac{d^3p'}{p_0'} = \frac{d^3p}{p_0}, \tag{2.8}$$

demonstrating that the "operator" $\int dP$ in (2.1) is also invariant.

Note that in quantum mechanics, it is also common to divide the phase space volume element by an explicit factor of h^3 [8]. Introducing a factor g which takes into account the degeneracy of states with "internal" quantum numbers of a particle species, we can write the number of all available quantum states in the phase space volume element as

$$g \frac{d^3x d^3p}{h^3}.$$

Fermions obey the Pauli exclusion principle, which states that two particles cannot occupy the same state (whilst any number of bosons can occupy the same state). For fermions, we can state that the phase space is completely occupied when the number of particles is equal to the number of available states $f = g/h^3$.[1]

For gluons we have g_{gluon} = (colour $\times$ spin)= $(8 \times 2) = 16$ and quarks g_{quark} =((quarks + antiquarks) $\times$ colour $\times$ spin $\times$ flavours)= $(2 \times 3 \times 2 \times N_f) = \frac{21}{2} N_f$, where N_f are the number of "active" quark flavours.

2.3 Macroscopic properties

In order to move from a microscopic description in terms of the distribution function to a macroscopic one, we compute certain moments of the distribution function by integrating over momentum space [11, 25]. The rank-n tensor which contains all the n-th order moments of the distribution function is defined as

$$M^{\alpha_1 \alpha_2 \ldots \alpha_n}(\mathbf{x}, t) = \int dP \prod_{i=1}^{n} p^{\alpha_n} f(\mathbf{x}, \mathbf{p}, t). \tag{2.9}$$

These are indeed Lorentz tensors since $\int dP$ and f are invariant (See section 2.22). Of particular interest are the first and second moments, which correspond to the particle four current $J^\alpha = \int dP p^\alpha f$ and energy-momentum tensor $T^{\alpha\beta} = \int dP p^\alpha p^\beta f$ which in general depend on t and $\mathbf{x}$ (See Section 2.3.2 and 2.3.3).

The energy-momentum tensor contains all the macroscopic information about the systems' energy and momentum densities and fluxes, while the four-current gives the particle density and the corresponding particle flux.

Along with the preceding definitions comes the notion of the collective velocity of the medium, as we explain in the following.

[1] This must be kept in mind when constructing an off-equilibrium initial condition for fermions. If we were to ignore this requirement, we can see in Appendix B that the number of vacant states $(1 - h^3/gf)$ would become negative, leading to a non-physical entropy current (2.23).

2.3.1 Fluid velocity

The collective velocity of the fluid u^α helps us define the local rest frame in which it is particularly simple to define local equilibrium. The fluid velocity is written as $u^\alpha = \gamma(1, \mathbf{u})$, where the local rest frame is defined by $u^\alpha_{LRF} = (1, \mathbf{0})$. In a relativistic setting, there are two ways to define the local rest frame [25]. The first choice is known as Eckart's rest frame, defined by vanishing particle flux,

$$J^\alpha_{LRF} = (\mathcal{N}_{LRF}, \mathbf{0}) \tag{2.10}$$

where $\mathcal{N}_{LRF}$ is the rest frame particle density, which is related to the four current in an arbitrary frame

$$\mathcal{N}_{LRF} = u_\alpha J^\alpha, \tag{2.11}$$

The second choice is the Landau-Lifschitz rest frame defined by vanishing energy flux, which can be expressed by the eigenvalue equation

$$u_\alpha T^{\alpha\beta} = \mathcal{E}_{LRF} u^\beta, \tag{2.12}$$

where $\mathcal{E}_{LRF}$ denotes the rest frame energy density. Since u^α must be time-like, we have the normalization $u_\alpha u^\alpha = 1$, thus the rest frame energy density can also be expressed by $\mathcal{E}_{LRF} = u_\alpha u_\beta T^{\alpha\beta}$.

Note that for an out-of-equilibrium fluid, the flow velocity u^α is not uniquely defined, since the rest frame in which the flow of particles (2.11) and the flow of energy (2.12) vanish do not agree in general. However, in local equilibrium, both choices of flow velocity become equivalent.

We exclusively make use of the Landau-Lifschitz choice (2.12) as energy conservation is universal, whilst we might consider particle number being conserved or not.

2.3.2 Energy-Momentum Tensor

The energy-momentum (EM) tensor

$$T^{\alpha\beta}_{[f]}(\mathbf{x}, t) = \int dP p^\alpha p^\beta f(\mathbf{x}, \mathbf{p}, t), \tag{2.13}$$

is the symmetric rank-2 tensor of second moments of the distribution function.

The energy-momentum tensor has a particularly interesting form when the distribution function f is isotropic in momentum space, in its local rest frame. In this case the distribution has the form $f \equiv f(p^\alpha u_\alpha)$ in an arbitrary frame. This implies that, in the local rest frame of the fluid, the energy-momentum tensor is completely characterized by the rest frame energy density $\mathcal{E}_{LRF}$ and the isotropic pressure $\mathcal{P}_{LRF}$

$$\mathcal{E}_{LRF} = \frac{g}{2\pi^2}\int_0^\infty dp p^2\sqrt{p^2+m^2}f(p), \qquad \mathcal{P}_{LRF} = \frac{g}{6\pi^2}\int_0^\infty dp\frac{p^4}{\sqrt{p^2+m^2}}f(p), \tag{2.14}$$

where $p = |\mathbf{p}|$. We have $T^{\alpha\beta}_{LRF} = \mathrm{diag}(\mathcal{E}_{LRF}, \mathcal{P}_{LRF}, \mathcal{P}_{LRF}, \mathcal{P}_{LRF})$, with all off-diagonal components vanishing by symmetry. In an arbitrary frame we can find the corresponding energy-momentum tensor by boosting [25]

$$T^{\alpha\beta}_{ideal} = \mathcal{E}_{LRF}u^\alpha u^\beta - \mathcal{P}_{LRF}\Delta^{\alpha\beta}, \tag{2.15}$$

where $\Delta^{\alpha\beta}$ is the so-called projector tensor specified in Appendix A. This is the energy-momentum tensor of a perfect fluid in which all viscous effects are absent. This form arises purely as a result of the momentum isotropy of f in the local rest frame. In particular, since the equilibrium distribution to be defined in (2.25) is isotropic in the rest frame, the corresponding energy-momentum tensor is of the form (2.15).

More generally, the distribution function is of course not limited to a local equilibrium form, and accordingly its energy-momentum tensor may be decomposed into perfect fluid (ideal) and dissipative parts [15, 8]

$$T^{\alpha\beta} = T^{\alpha\beta}_{ideal} + \Pi^{\alpha\beta}, \tag{2.16}$$

where $T^{\alpha\beta}_{ideal}$ is the perfect fluid contribution in (2.15). The contribution $\Pi^{\alpha\beta}$ can be further decomposed into trace-free part $\pi^{\alpha\beta}$ and the remainder $\Pi\Delta^{\alpha\beta}$. This decomposition lets us interpret the physical meaning of the various components of $T^{\alpha\beta}$. From the definition of our fluid velocity (2.12), we infer that $u_\alpha\Pi^{\alpha\beta} = 0$. The tensor $\pi^{\alpha\beta}$ contains all the shear stresses. We have that it is traceless, $\pi^\alpha_\alpha = 0$, symmetric, $\pi^{\alpha\beta} = \pi^{\beta\alpha}$, and transverse, $u_\alpha\pi^{\alpha\beta} = 0$. Π is the bulk viscous pressure which can be inferred from the properties of

the projector $\Delta^{\alpha\beta}$ detailed in Appendix A.

The viscous shear tensor $\pi^{\alpha\beta}$ and bulk viscous tensor $\Pi^{\alpha\beta}$ both play an important role in the derivation of Hydrodynamics away from the ideal (perfect fluid) limit [15, 24].

Note that for massless particles $p^\alpha p_\alpha = 0$, which implies that the EM tensor is traceless $T^\alpha_\alpha = 0$, thus the relationship $\mathcal{E} = 3\mathcal{P}$ for the ideal gas holds even out of equilibrium. Furthermore, if we write the dissipative part of the distribution function as δf, and use $\Delta^\alpha_\alpha = 3$ from Appendix A, we have

$$\Pi^\alpha_\alpha = \Pi\Delta^\alpha_\alpha = \frac{1}{3}\int dP p^\alpha p_\alpha \delta f, \tag{2.17}$$

which vanishes identically since $p^\alpha p_\alpha = 0$. Consequently, the massless system does not have a bulk viscous pressure.

2.3.3 Four-Current

The four-current

$$J^\alpha_{[f]}(\mathbf{x}, t) = \int dP p^\alpha f(\mathbf{x}, \mathbf{p}, t), \tag{2.18}$$

is a rank-1 tensor formed of first moments of the distribution function [25].

As with the energy-momentum tensor, for a distribution which is isotropic in its local rest frame, the four-current takes a particular form

$$J^\alpha_{ideal} = \mathcal{N}_{LRF} u^\alpha, \tag{2.19}$$

where the rest frame particle density $\mathcal{N}_{LRF} = \sqrt{J^\alpha J_\alpha}$, since $u^\alpha u_\alpha = 1$. The rest frame particle density can be written as

$$\mathcal{N}_{LRF} = \frac{g}{2\pi^2}\int_0^\infty dp p^2 f(p). \tag{2.20}$$

In general we can decompose

$$J^\alpha = J^\alpha_{ideal} + V^\alpha, \tag{2.21}$$

where V^α can be interpreted as a heat flux satisfying $u_\alpha V^\alpha = 0$ [8].

2.3.4 Entropy Four-Current

The entropy is a sensitive measure of the degree of equilibration of the system, since the Boltzmann equation obeys the second law of thermodynamics. In relativistic form the second law reads [8, 25]

$$\partial_\alpha S^\alpha \geq 0, \tag{2.22}$$

where S^α is the entropy current. This states that the invariant entropy production rate must not be negative. Note that this rate vanishes only in equilibrium, which is the state of maximal entropy.

Whilst $T^{\alpha\beta}$ and J^α are independent of the quantum nature of particles, the entropy four-current S^α assumes a different form based on the type of particles under consideration. This is a reflection of the fact that bosons and fermions obey different statistics.

In a unifying notation [25]

$$S^\alpha = -\int dP p^\alpha (f \ln f - \frac{1}{\epsilon} \bar{f} \ln \bar{f}), \tag{2.23}$$

where $\bar{f} \equiv 1 + \epsilon f$ and $\epsilon = \{1, -1\}$ for bosons or fermions, respectively, whereas $\epsilon \to 0$ formally describes the classical limit which is

$$S^\alpha = -\int dP p^\alpha (f \ln f - 1). \tag{2.24}$$

In Appendix B, we show that H-theorem (2.22) indeed holds for the Boltzmann equation in the relaxation time approximation (2.32).

2.4 Local Equilibrium

The equilibrium distribution for a particular species of particle is the distribution for which the entropy production (2.22) vanishes. For bosons this is the Bose-Einstein (BE) distribution, fermions the Fermi-Dirac (FD) distribution and the Maxwell Boltzmann (MB) distribution is for classical particles. The relativistic forms of these distributions are known as the Jüttner distributions [25, 8]

$$f(\mathbf{x}, \mathbf{p}) = \frac{1}{\exp[(p^\alpha u_\alpha(\mathbf{x}) - \mu(\mathbf{x}))/T(\mathbf{x})] - \epsilon}, \tag{2.25}$$

where $\epsilon = \{1, -1, 0\}$ for Bosons, Fermions and Maxwell Boltzmann particles, respectively, and $u^\alpha = \gamma(1, \mathbf{u})$ is the relativistic four velocity of the fluid. Furthermore T is the temperature and μ the chemical potential all of which can depend on the position. The chemical potential only appears if particle number is conserved (see Section 2.5). Note that in the local rest frame of the fluid where $u^\alpha = (1, \mathbf{0})$ and $p^\alpha u_\alpha = p_0$, the distribution depends only on the equilibrium parameters $\{T, \mu\}$. This implies that is isotropic in momentum space, and thus has a four-current and energy-momentum tensor of the forms (2.19) and (2.15).

In this thesis, we work predominantly with massless bosons. Using equations (2.14) and (2.20) and substituting the BE distribution of massless bosons we have for the equilibrium particle (2.20) and energy density (2.14) in the rest frame

$$\mathcal{N}_\infty(\mathbf{x}) = \frac{g}{\pi^2}\mathrm{Li}_3(e^{\frac{\mu}{T}})T^3, \qquad \mathcal{E}_\infty(\mathbf{x}) = \frac{3g}{\pi^2}\mathrm{Li}_4(e^{\frac{\mu}{T}})T^4, \tag{2.26}$$

where $\mathrm{Li}_s(z)$ is the polylogarithm of order s and argument z (see Appendix A), and the gluon degeneracy $g = 16$. Note the special cases $\mathrm{Li}_3(1) = \zeta(3) \approx 1.2$ and $\mathrm{Li}_4(1) = \pi^4/90 \approx 1.08$, which correspond to a vanishing chemical potential $\mu = 0$.

2.5 Bose-Einstein Condensation

We wish to describe the dynamics of an initially out-of-equilibrium system towards an equilibrium state. The final equilibrium state uniquely depends on the initial state. In particular it is constrained by the conservation of energy and any other conserved charges.

Consider as a special case, a closed homogeneous system in the local rest frame where momentum and particle fluxes vanish. If the system conserves only energy (and not particle number), the temperature of the corresponding equilibrium state is entirely determined by the energy-momentum tensor of the initial system. For a system where particle number is also conserved, we must introduce a finite chemical potential. For a gluon system, such as the one we are interested in, the concept of a gluon chemical potential may be justified in a certain time window, which may even be large enough to approach equilibrium. In this case, interactions are dominated by elastic $2 \to 2$ scatterings whereas number changing

(inelastic) processes are subdominant. This picture may be applicable in the early stages of a heavy ion collision, after the CGC state [14] and before the system thermalizes and hydrodynamics becomes applicable. For very long times, number changing processes will dominate, which drives the gluon chemical potential to zero.

In order to shed some light on the role of the Bose-Einstein condensate, consider a system of massless bosons in a homogeneous box, in equilibrium. If we assume that the number of particles remains fixed and begin to slowly reduce the temperature of the system through external cooling, the number of particles needs to be regulated through a finite negative chemical potential μ, which according to (2.26) must increase to compensate for the reduction in temperature. However, we strictly cannot have $\mu > 0$ since the BE distribution would then become negative in regions of phase space where $p < \mu$. The result is that below a critical temperature, the bosons begin to populate the lowest energy state, as they can no longer be supported by a thermal distribution. This signifies a phase transition into the Bose-Einstein condensate. The equilibrium distribution then becomes [5]

$$f_\infty(\mathbf{p}) = \frac{1}{\exp(p/T) - 1} + (2\pi)^3 n_c \delta(\mathbf{p}). \tag{2.27}$$

The additional term $f_c = (2\pi)^3 n_c \delta(\mathbf{p})$ is normalized so as to give $\int dP f_c = n_c$, where n_c is the density of condensate particles. Since particles in the condensate have zero momentum by definition, the extra term does not contribute to the energy-momentum tensor $\int dP p^\alpha p^\beta f_c = 0$.

In the context of the Boltzmann equation we are interested in whether a Bose-Einstein condensate can form dynamically in heavy ion collisions. Such a situation may arise when particle conserving processes dominate – as assumed previously – and the initial state contains sufficiently many particles. In this setting, rather than the temperature being too low for a certain number of particles, the gluon densities in the early stages of the collision are too high compared with the corresponding energy density (in the local rest frame) [5].

On the other hand, if particle conserving processes are absent, we fix $\mu = 0$ and the particle number will then begin to preferentially decrease or increase "instantaneously"

to asymptotically fit the thermal distribution as it is brought into equilibrium, thereby precluding the existence of a condensate. The physical situation will lie somewhere between the two extreme assumptions.

To quantify how "dense" a system needs to be, we follow [5]. First, we introduce the dimensionless parameter $\chi = \mathcal{N}/\mathcal{E}^{3/4}$ which characterizes the overpopulation of the system. In equilibrium at $\mu = 0$ from (2.26) we have

$$\mathcal{N}_\infty = \frac{g}{\pi^2}\zeta(3)T^3, \qquad \mathcal{E}_\infty = \frac{g\pi^2}{30}T^4, \tag{2.28}$$

and therefore $\chi_\infty = \mathcal{N}_\infty/\mathcal{E}_\infty^{3/4} = 30^{3/4}\zeta(3)g^{1/4}/\pi^{7/2} \approx 0.28g^{1/4}$ (≈ 0.56 for gluons). Systems with $\chi > \chi_\infty$ are called overpopulated, and will lead to the formation of a Bose-Einstein condensate when particle conserving processes dominate. A system with $\chi < \chi_\infty$ is called underpopulated and can be entirely accommodated by the BE distribution with a finite and negative chemical potential μ. At $\mu = 0$ the system is thermally distributed.

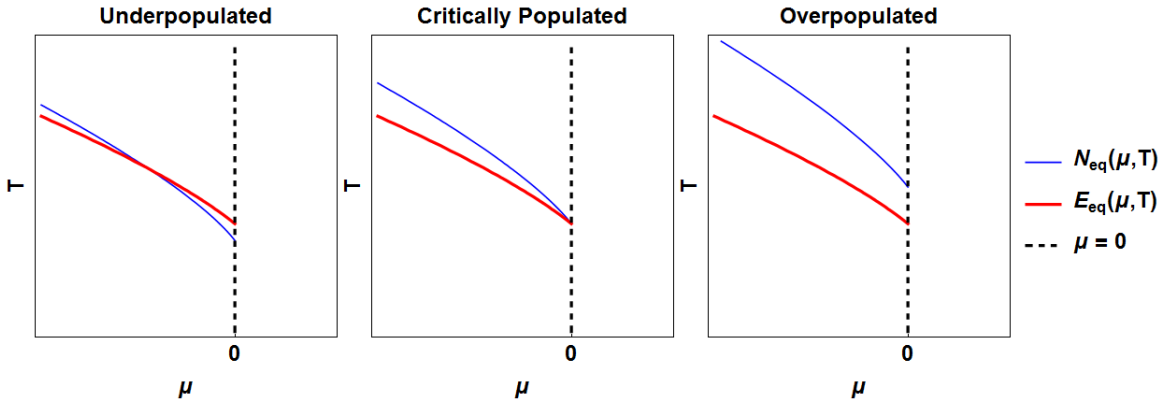

Figure 2.1: Contours of constant $\mathcal{N}_\infty(\mu, T)$ and $\mathcal{E}_\infty(\mu, T)$ for the three possible scenarios. The equilibrium parameters $\{\mu_\infty, T_\infty\}$ are found at their intersection. For a given energy density, particle number is increased resulting in a corresponding increase of μ_∞ until a critical point at $\mu_\infty = 0$. A further increase in particle number yields contours which do not overlap in the physical region $\mu < 0$. These additional particles may be stored in the condensate.

In order to describe on the same footing both the underpopulated and overpopulated regime, let us introduce a dimensionful parameter ν which is related to either the chemical potential μ or the condensate density n_c

$$f_\infty(\mathbf{p}, \nu, T) = \frac{1}{\exp((p - \mu(\nu))/T) - 1} + (2\pi)^3 n_c(\nu)\delta(\mathbf{p}), \tag{2.29}$$

where

$$\mu(\nu) = \begin{cases} \nu, & \nu \leq 0 \\ 0, & \nu > 0 \end{cases} \tag{2.30}$$

and

$$n_c(\nu) = \begin{cases} 0, & \nu \leq 0 \\ \nu^3, & \nu > 0 \end{cases} \tag{2.31}$$

This enables us to explore all regions of the "phase space" $\{T, \nu\}$.

2.6 Relaxation time approximation

The covariant form of the relaxation time approximation was first introduced by J.L. Anderson and H.R. Witting [2]. It is a relativistic extension of the BGK (Bhatnagar, Gross and Krook) equation[8]. Both are models designed to capture certain features of the full Boltzmann equation. It is stated as [2, 11]

$$p^\alpha \partial_\alpha f(\mathbf{x}, \mathbf{p}) = p^\alpha u_\alpha \frac{f_\infty(\mathbf{x}, \mathbf{p}) - f(\mathbf{x}, \mathbf{p})}{\tau_{rel}}, \tag{2.32}$$

where u_α is the flow velocity defined by the Landau-Lifschitz choice (2.12), where the energy flux vanishes in the rest frame of the fluid. The function f_∞ is the relevant equilibrium Jüttner distribution (2.25),(2.27), which depends on the quantum nature of the particles under consideration.

Whilst at first glance equation (2.32) appears linear, it must be noted that the equilibrium distribution f_∞ in fact depends in a non-linear way on the distribution function f at a given time through its equilibrium parameters $\{T, \nu\}$ – which in turn are calculated from integrals of the distribution function over the full momentum space. This means that the relaxation time collision term is also non-local in momentum space.

The set of relevant moments of the distribution function, correspond to the particle four-current and energy-momentum tensor of the system respectively.

The equilibrium parameters are determined by the energy-momentum tensor and in the case of particle conservation, the particle four-current. In covariant form the equations

for conservation of energy-momentum and particle number read

$$\partial_\alpha T^{\alpha\beta}(\mathbf{x}) = 0, \tag{2.33}$$

$$\partial_\alpha J^{\alpha}(\mathbf{x}) = 0, \tag{2.34}$$

Using the Boltzmann equation in the relaxation time approximation (2.32), and introducing the notation $T^{\alpha\beta}_{[f_\infty]} = T^{\alpha\beta}_{\infty}$ we can specify the conservation equations as

$$\begin{aligned}
\partial_\alpha T^{\alpha\beta}_{[f]} &= \partial_\alpha \int dP p^\alpha p^\beta f(\mathbf{x},\mathbf{p}) \\
&= \int dP p^\beta p^\alpha \partial_\alpha f(\mathbf{x},\mathbf{p}) \\
&= \int dP p^\beta p^\alpha u_\alpha \frac{f_\infty(\mathbf{x},\mathbf{p}) - f(\mathbf{x},\mathbf{p})}{\tau_{rel}} \\
&= u_\alpha (T^{\alpha\beta}_{\infty} - T^{\alpha\beta}_{[f]})/\tau_{rel},
\end{aligned} \tag{2.35}$$

and similarly for J^α

$$\begin{aligned}
\partial_\alpha J^{\alpha}_{[f]} &= \partial_\alpha \int dP p^\alpha f(\mathbf{x},\mathbf{p}) \\
&= \int dP p^\alpha \partial_\alpha f(\mathbf{x},\mathbf{p}) \\
&= \int dP p^\alpha u_\alpha \frac{f_\infty(\mathbf{x},\mathbf{p}) - f(\mathbf{x},\mathbf{p})}{\tau_{rel}} \\
&= u_\alpha (J^{\alpha}_{\infty} - J^{\alpha}_{[f]})/\tau_{rel}.
\end{aligned} \tag{2.36}$$

Since we require the right hand sides to vanish, we obtain the conditions

$$u_\alpha T^{\alpha\beta}_{[f]} = u_\alpha T^{\alpha\beta}_{\infty}, \tag{2.37}$$

and

$$u_\alpha J^{\alpha}_{[f]} = u_\alpha J^{\alpha}_{\infty}. \tag{2.38}$$

Making use of the isotropy of f_∞ through (2.15), (2.19) and $u^\alpha u_\alpha = 1$, these can be further simplified to

$$u_\alpha u_\beta T^{\alpha\beta}_{[f]} = \mathcal{E}_\infty(T,\nu), \qquad u_\alpha J^{\alpha}_{[f]} = \mathcal{N}_\infty(T,\nu). \tag{2.39}$$

The first expression in (2.39) is a set of four equations that lets us specify $\{T, \mathbf{u}\}$ the temperature and the three independent components of the flow velocity for $f_\infty(T,\mathbf{u})$ in

a manner which conserves both energy and momentum of the system. If we wish to consider processes which also conserve particle number, a finite chemical potential μ and/or n_c which appears in the equilibrium distribution $f_\infty(T, \mathbf{u}, \nu)$ can be fixed with the second expression in (2.39).

The relaxation time approximation (2.32) is expected to appropriately reproduce essential features of the full Boltzmann equation with a realistic collision term [8]. In order to justify this expectation, we study the so-called summational invariants. These are a class of continuous, differentiable functions of the form $\psi = a + B^\alpha p_\alpha$ where a and B_α are an arbitrary Lorentz scalar and four-vector independent of the four-momentum p^α. These functions are related to the equilibrium distributions and follow as a consequence of the conservation of energy and particle number.

For both bosons and fermions, using the equilibrium distribution (2.25) we have

$$\ln \frac{f_\infty}{\bar{f_\infty}} = \frac{u^\alpha p_\alpha - \mu}{T}, \tag{2.40}$$

where $\bar{f_\infty} = 1 + \epsilon f_\infty$. This is readily seen to be a summational invariant by identifying $a = -\mu/T$ and $B^\alpha = u^\alpha/T$.

We expect both the true collision term and equation (2.32) to satisfy the following[8]:

1. For all summational invariants $\psi = a + B_\alpha p^\alpha$:

$$\int dP \psi C_{[f]} = 0. \tag{2.41}$$

2. The Boltzmann H-theorem:

$$\partial_\alpha S^\alpha \geq 0. \tag{2.42}$$

In addition to the two properties above, the collision term and therefore the entropy production rate vanish when the system is in equilibrium, i.e. $f = f_\infty$,

$$C_{[f_\infty]} = p^\alpha u_\alpha (f_\infty - f_\infty)/\tau = 0, \tag{2.43}$$

therefore

$$\begin{aligned}\partial_\alpha S^\alpha(f_\infty) &= \int dP \ln\frac{f}{\bar{f}} p^\alpha \partial_\alpha f_\infty \\ &= \int dP \ln\frac{f}{\bar{f}} p^\alpha C_{[f_\infty]} \\ &= 0. \end{aligned} \tag{2.44}$$

Boltzmann relaxation for an isotropic homogeneous system

In order to gain insight into the physics of the Boltzmann equation (2.32), here we neglect convective effects ($p^\alpha\partial_\alpha \to p_0\partial_t$) and work in the local rest frame ($p^\alpha u_\alpha \to p_0$). This describes a system in a homogeneous box, with an isotropic momentum distribution. In this simplified scenario we have

$$\partial_t f = \frac{f_\infty - f}{\tau_{rel}}, \tag{2.45}$$

and the conservation laws to fix the equilibrium parameters (2.39) reduce to $T^{00}_{[f_0]} = T^{00}_\infty$, $T^{0i}_{[f_0]} = T^{0i}_\infty = 0$, and $J^0_{[f_0]} = J^0_\infty$.

While different momentum modes should evolve on different timescales, it is generally assumed that τ_{rel} in (2.32) is constant [10, 15]. Under this assumption, the solution to (2.32) is obviously

$$f(t) = f_\infty + (f_0 - f_\infty)e^{-t/\tau_{rel}}, \tag{2.46}$$

for a given initial distribution f_0. So, the distribution f asymptotically approaches the equilibrium form f_∞ from an initial state f_0, at a rate controlled by the relaxation time parameter τ_{rel}.

The energy-momentum tensor and particle-current evolve as

$$T^{\alpha\beta}(t) = T^{\alpha\beta}_\infty + (T^{\alpha\beta}_{[f_0]} - T^{\alpha\beta}_\infty)e^{-t/\tau_{rel}}, \tag{2.47}$$

$$J^\alpha(t) = J^\alpha_\infty + (J^\alpha_{[f_0]} - J^\alpha_\infty)e^{-t/\tau_{rel}}, \tag{2.48}$$

which asymptotically approach the perfect fluid forms (2.15) and (2.19). Consequently the viscous contributions $\Pi^{\alpha\beta} = \Pi^{\alpha\beta}_0 e^{-t/\tau}$ and $V^\alpha = V^\alpha_0 e^{-t/\tau}$ in (2.16) and (2.21) approach zero.

Dynamic equilibrium

The solution (2.46) applies to an isotropic system in a homogeneous box $f = f(|\mathbf{p}|)$. Note that this solution follows from the assumption that f_∞ does not change in time. However this need not be the case and we would in general expect the equilibrium parameters to change as a function of time for initial distributions that deviate from this isotropy.

This seems plausible since we have unconstrained parameters. The energy-momentum tensor has in general $(16 - 6 - 1 = 9)$ independent components due to being both symmetric ($T^{\alpha\beta} = T^{\beta\alpha}$) and traceless ($T^\alpha_\alpha = 0$), but we have only 4 equations (2.39) with which to fix $\mathcal{E}_\infty$ and $\mathbf{u}$. If particle number is also conserved, the four-current J^α introduces 4 additional independent components, with a single equation (2.39) to fix $\mathcal{N}_\infty$.

However, as illustrated in Figure 2.2 we can always predict the "asymptotic" equilibrium state that the system will approach in long times. We can do so since we strictly have $\partial_t T^{0\alpha} = 0$ and (if we conserve particle number) $\partial_t J^0 = 0$ in a homogeneous setting. These are $4 + 1$ equations over $4 + 1$ parameters which uniquely specify the asymptotic equilibrium parameters from the initial state.

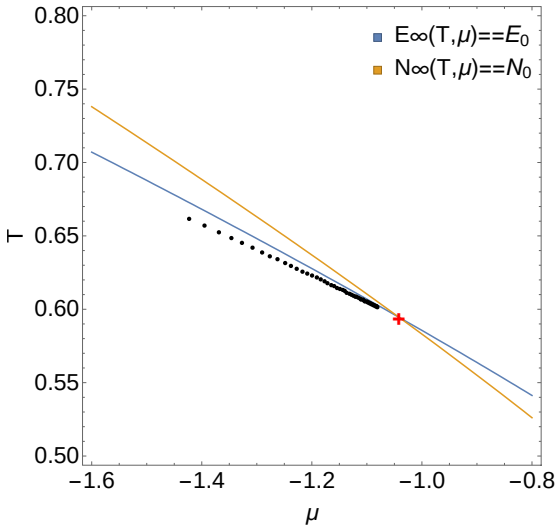

Figure 2.2: Numerical evolution of equilibrium parameters for a 2D system in a homogeneous box with a finite flow $\mathbf{u}$, for an off-equilibrium initial condition $f_0(p_x, p_y) = 0.1 \exp[-((p_x + 1.7)^2 + (p_y + 1.2)^2)/2]$. The solid curves are the predicted energy and particle densities of the asymptotic equilibrium. The black dots represent the parameters determined by (2.39) and (2.26) at each time step, which evolve in time towards the asymptotic value indicated by the red cross.

Estimating the relaxation time

Throughout the rest of this thesis, we assume the relaxation time τ_{rel} appearing in (2.32) is a constant throughout space-time and momentum, but note that generally speaking this is not the case [13]. Realistically the relaxation time for a pure gluon plasma in QCD can be determined by [2]

$$\tau_{rel} = \frac{1}{\mathcal{N}\sigma_t}, \tag{2.49}$$

where $\mathcal{N}$ is the particle density and

$$\sigma_t = \int_{-s}^{-\mu^2} dt \frac{d\sigma}{dt} \frac{|t|}{s}, \tag{2.50}$$

is the so-called transport cross section where s and t are the usual Mandelstam variables and μ is an infrared cutoff. The quantities in (2.49) are expected to change throughout the evolution of the Boltzmann equation (2.32) due to "convective" effects.

Let us estimate τ_{rel} according to QCD. To tree level accuracy we have [21]

$$\frac{d\sigma}{dt} \simeq 9\pi \frac{\alpha^2}{t^2}, \tag{2.51}$$

wheres α is the QCD coupling constant. The transport cross section therefore becomes

$$\begin{aligned} \sigma_t &= \frac{9\pi\alpha^2}{s} \int_{-s}^{-\mu^2} \frac{dt}{|t|} \\ &= \frac{9\pi\alpha^2}{s} \ln \frac{s}{\mu^2} \\ &\approx \frac{9\pi\alpha^2}{s}, \end{aligned} \tag{2.52}$$

where in the final step we approximate the Coulomb logarithm $\ln(s/\mu^2) \approx \ln(1/\alpha) \approx 1$ [21]. The typical value of s in the relativistic limit can be estimated as $s \approx 2(\mathcal{E}/\mathcal{N})^2 \approx 2(2.7T)^2$. Furthermore, recall for a thermalized gluon system the particle density (2.26) is $\mathcal{N} = \frac{16\times 4\pi}{(2\pi)^2}\zeta(3)T^3 \approx 2T^3$. Therefore the relaxation time

$$\begin{aligned} \tau_{rel}^{-1} = \mathcal{N}\sigma_t &\approx (2T^3)\left(\frac{9\pi\alpha^2}{2(2.7T)^2}\right) \\ &\approx 4\alpha^2 T. \end{aligned} \tag{2.53}$$

[2] Additionally, a factor of the average relative velocity $\bar{v}$ should feature in the denominator. However, for an ultra-relativistic gas $\bar{v} \approx c = 1$ in our system of units.

At a relevant temperature of, say, $T = 300$ MeV the typical QCD coupling is of the order of 0.5. We therefore expect from (2.53) that τ_{rel} is of the order of 1 fm.

We can alternatively gain a quick estimate of τ_{rel} by looking at the time scales involved in a heavy ion event. In this situation, the system approaches a near-to-equilibrium state in a time range between $2 - 10$ fm/c [15, 14]. In the relaxation time approximation the distribution f is closer to the equilibrium f_∞ by a factor of e for each multiple of the relaxation time. This means from about $t \approx 5\tau_{rel}$, the system is approximately in equilibrium. This suggests our relaxation time must lie approximately in the range $\tau \approx 0.5 - 2$ fm/c, in agreement with the estimate due to QCD above.

2.6.1 Bjorken Expansion

In a heavy ion event, nuclei approach each other at near-to-light speeds along the beam pipe and do not have much stopping power. As a result, the nuclei typically pass through each other, maintaining a longitudinal momentum much larger than their transverse momentum. Due to this large scale separation, there is a strong correlation between the typical longitudinal momentum and the space time coordinates. For instance, a particle with speed v_z will be found in a definite region of space time given by $v_z = p_z/p_0 \approx z/t$. Furthermore, for a time shorter than the transverse size of the nucleus, the transverse expansion may be effectively neglected [24, 25].

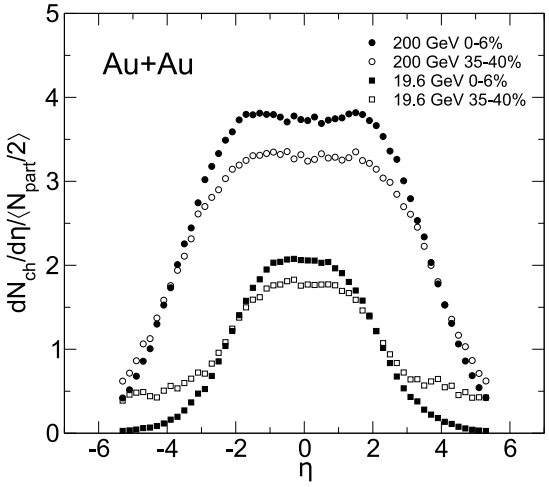

Figure 2.3: Charged particle production as a function of pseudo-rapidity for different beam energies in AuAu collisions. The flattened peaks are a reflection of the boost-invariant character of the system around the central rapidity $z \approx 0$ region. Figure due to [24].

The Bjorken model [4] assumes that the energy density of a system is uniform in space-time rapidity so that $\mathcal{E}(t, z) = \mathcal{E}(\tau)$ where $\tau = \sqrt{t^2 - z^2}$ is the proper time. Under this assumption, the correlation between the momentum and space time coordinates remains fixed, yielding a flow velocity of $u^\alpha = \gamma(1, 0, 0, z/t)$. The Bjorken model is invariant under longitudinal boosts.

Following [3, 5, 4], let us consider a system that is undergoing such longitudinal boost-invariant expansion. Consequently, we have that the distribution function at position z at time t is the same as that at the central slice $z = 0$ at proper time τ. We can then write $f(p_z, p_t, z, t) = f(p'_z, p_t, \tau)$ where $p'_z = \gamma(p_z - pu_z)$ is the boosted longitudinal momentum

and $u_z = z/t$.

These assumptions let us focus on the distribution on the central slice $z = 0$ and build up the full distribution by appropriate longitudinal boosts, greatly simplifying any analytic or numeric calculations.

On the central slice we have $\tau = t$ and by symmetry $u^\alpha = (1, 0, 0, 0)$. The calculation of the conservation laws to fix the equilibrium parameters (2.39) are then just that of an isotropic system: $T^{0\beta}_\infty = T^{0\beta}_{[f]}$ and $J^0_\infty = J^0_{[f]}$.

Furthermore, the Boltzmann equation (2.32) becomes

$$\partial_t f - \frac{p_z}{t}\partial_{p_z} f = \frac{f_\infty - f}{\tau_{rel}}. \tag{2.54}$$

since we have $p^\alpha u_\alpha = p_0$ and $v_z \partial_z = -\frac{p_z}{t}\partial_{p_z}$.

The evolution equations for the energy density and particle density in the central slice at $z = 0$ can be found by integration of (2.54) [3]. Noting that the collision term vanishes by the conservation laws, we obtain

$$\partial_t \mathcal{E} + \frac{\mathcal{E} + P_z}{t} = 0, \qquad \partial_t \mathcal{N} + \frac{\mathcal{N}}{t} = 0, \tag{2.55}$$

where $\mathcal{E} = \int dP p_0^2 f$ is the energy density at $z = 0$ and $P_z = \int dP p_z^2 f$ is the corresponding longitudinal pressure. The rate at which the energy flows out of the central slice is dependent on the pressure anisotropy through the appearance of P_z. Let us characterize this anisotropy through the parameter $\delta \in [0, 1/3]$[3] by setting $P_z = \delta\mathcal{E}$, then the solution to (2.55) is

$$\mathcal{E}(t) = \mathcal{E}\left(\frac{t_0}{t}\right)^{1+\delta}. \tag{2.56}$$

For the particle number we have

$$\mathcal{N}(t) = \mathcal{N}_0\left(\frac{t_0}{t}\right). \tag{2.57}$$

[3]These limits apply to an initially oblate configuration in momentum space where the transverse pressure is initially greater or equal to the longitudinal pressure, as is expected in a heavy ion event, shortly after the nuclei have passed through one another.

Note that δ is not fixed, but is expected to change in time due to collisions which seek to make the system isotropic $\delta \to 1/3$. Note however that the pressure isotropy $P_z = \mathcal{E}/3$ will be maintained in the limit of "infinite interactions" $\tau_{rel} \to 0$ which corresponds to a system undergoing ideal hydrodynamic expansion. On the other hand, $\tau_{rel} \to \infty$ corresponds to the free-streaming limit where $\delta = 0$ and therefore $P_z = 0$.

We can use these equations to gain insight into how the overpopulation parameter $\mathcal{N}/\mathcal{E}^{-3/4}$ – and therefore the Bose-Einstein condensate – changes as a result of the longitudinal expansion. The time dependence of the overpopulation parameter is

$$\mathcal{N}\mathcal{E}^{-3/4} \approx \left(\frac{t_0}{t}\right)^{(3\delta-1)/4}. \tag{2.58}$$

We then have two cases to consider: When $\delta < 1/3$ the parameter decreases in time and for $\delta = 1/3$, it remains unchanged. The first instance allows for a transient Bose-Einstein condensate, in the case of an overpopulated initial condition, whereas the second case will remain overpopulated. In the ideal hydrodynamic limit the condensate term can exist all the way up to thermalization. As usual, if we do not consider particle conservation, no condensate will form.

The preceding analysis indicates that the Bose-Einstein condensate is more likely to persist for longitudinal flow closer to the ideal hydrodynamic case. This is not surprising, since the stronger the interactions, the faster the system is brought into an isotropic momentum distribution. In the case of a system with an initial pressure anisotropy $P_z < P_\perp$ for example, this implies that transverse pressure $P_\perp$ is being converted into longitudinal pressure P_z, which in turn drives energy out of the central slice more efficiently.

We will first present some of our numerical results assuming this simplified geometry, and then continue with the implementation of the fully 3-Dimensional Boltzmann equation.

Results

We present some results for the 0+1 D Boltzmann equation undergoing longitudinal Bjorken expansion. We numerically solve (2.54) with the inclusion of the Bose-Einstein

condensate term (2.29). We implement an overpopulated Gaussian initial condition $f_0(p_\perp, p_z) = 100\exp(-(p_\perp^2 + \epsilon p_z^2))$ which is isotropic in transverse momentum $p_\perp$ (such as for a central collision) and we control the momentum isotropy between $p_\perp$ and p_z by the parameter ϵ. Shortly after two heavy ions collide and most of the matter has left the central slice $z = 0$, the typical transverse momentum is expected to be much larger than the longitudinal momentum [23] so we set $\epsilon = 100$. We choose an initial time $t_0 = 0.5$ fm/c and run the code until $t = 10$ fm/c for several different values of τ_{rel}. We compare this to the analytic results shown above due to [3, 5].

We consider four possible values for the relaxation time τ_{rel}: two moderate values $\tau_{rel} = 0.5$ fm/c and $\tau = 2$ fm/c, the free stream limit $\tau_{rel} \to \infty$ and the ideal hydrodynamic limit $\tau_{rel} \to 0$. We plot the evolution of the energy and particle densities assuming particle conservation, from $t = 0.5 - 10$ fm/c and note particularly how the condensate n_c evolves in time.

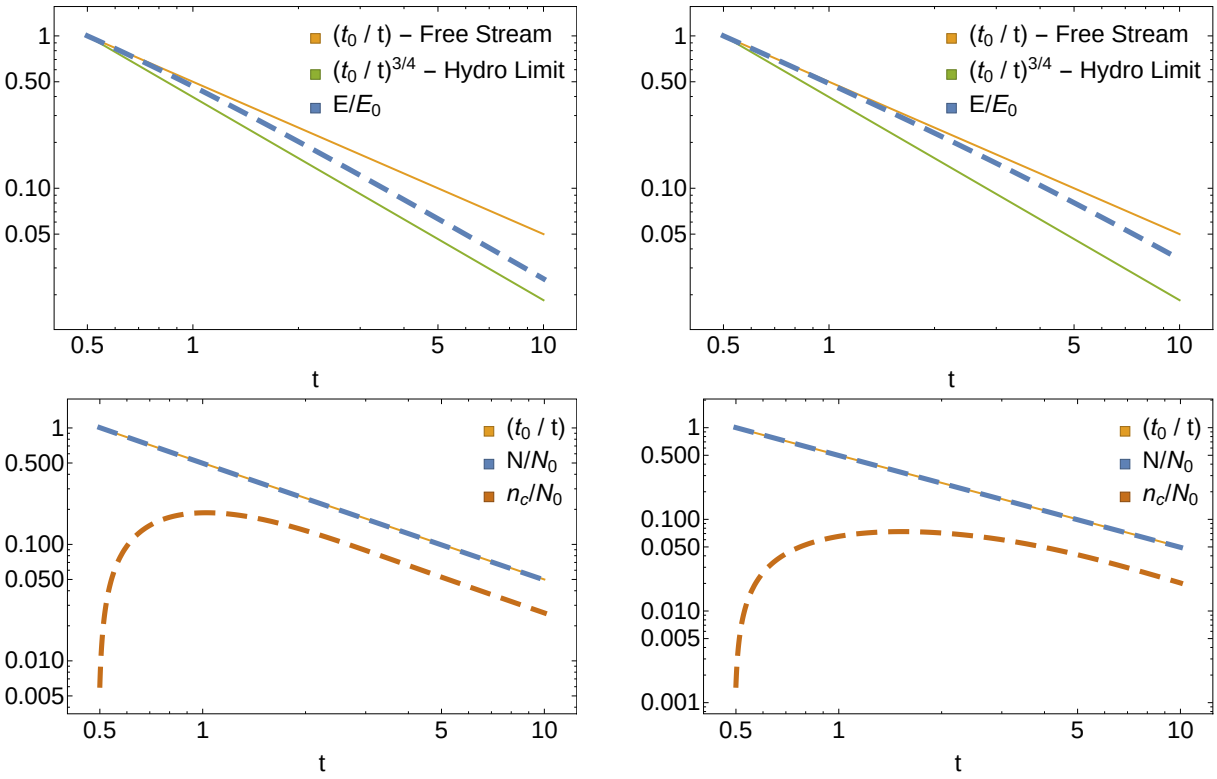

(a) $\tau_{rel} = 0.5$ fm/c (b) $\tau_{rel} = 2$ fm/c

Figure 2.4: Time evolution of the energy and particle densities in the central $z = 0$ slice for moderate values of the relaxation time τ_{rel}. The approach to condensation is faster for smaller τ_{rel}.

In Figure 2.4 we see that the evolution of the energy density lies between the two limiting cases in (2.56) where $\delta = 0$ and $\delta = 1/3$ as expected. The smaller the relaxation time, the faster the energy flows out of the central slice $z = 0$ and the faster the system is driven towards condensation.

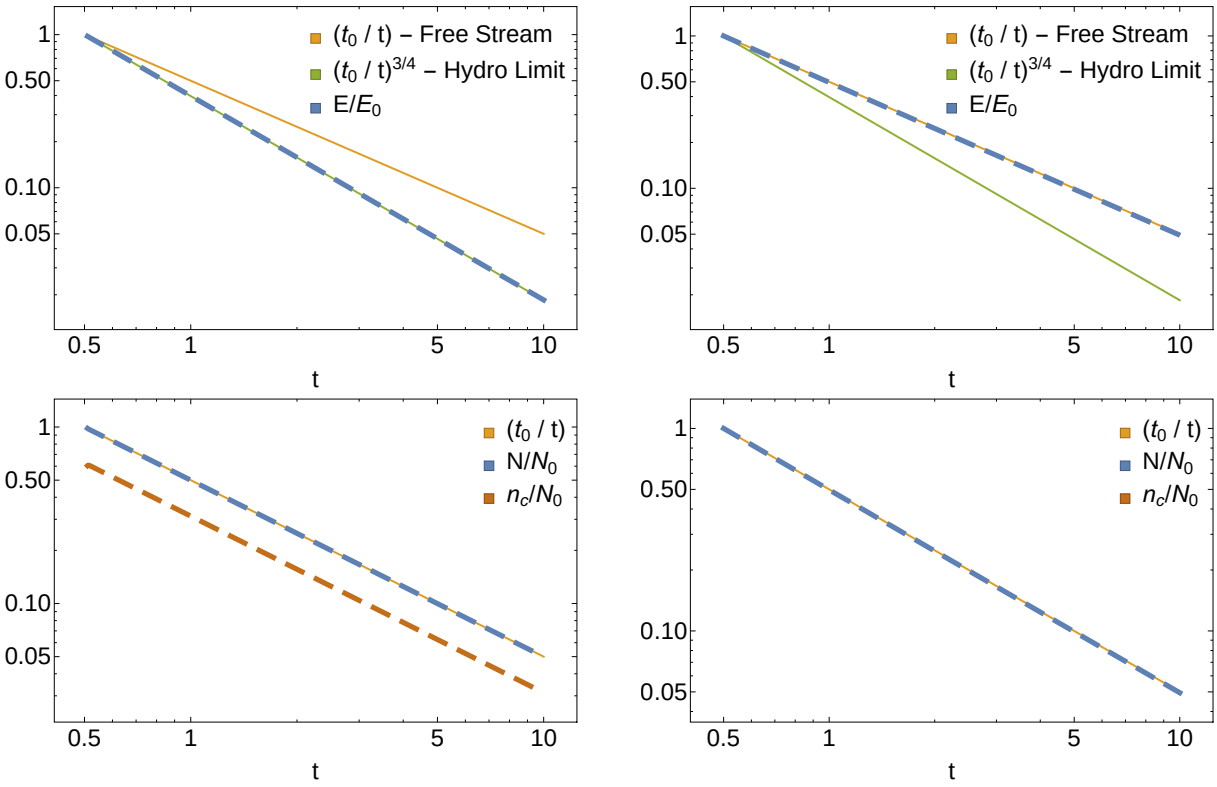

(a) $\tau_{rel} \to 0$ fm/c (b) $\tau_{rel} \to \infty$ fm/c

Figure 2.5: Time evolution of the energy and particle densities in the central $z = 0$ slice for the limiting cases of the relaxation time τ_{rel}. Near to the ideal Hydrodynamic limit (a), the approach to condensation is almost instantaneous, whilst in the free streaming limit (b), no condensate builds up.

In Figure 2.5 we show the evolution of the various quantities for the two limiting cases. We can see that the energy density matches the evolution in the two limiting cases obtained analytically. In the free stream limit the condensate does not build up at all, signifying the absence of interactions. Near the hydrodynamic limit on the other hand, the condensate builds up almost instantaneously and contains the largest number of particles of the cases shown here.

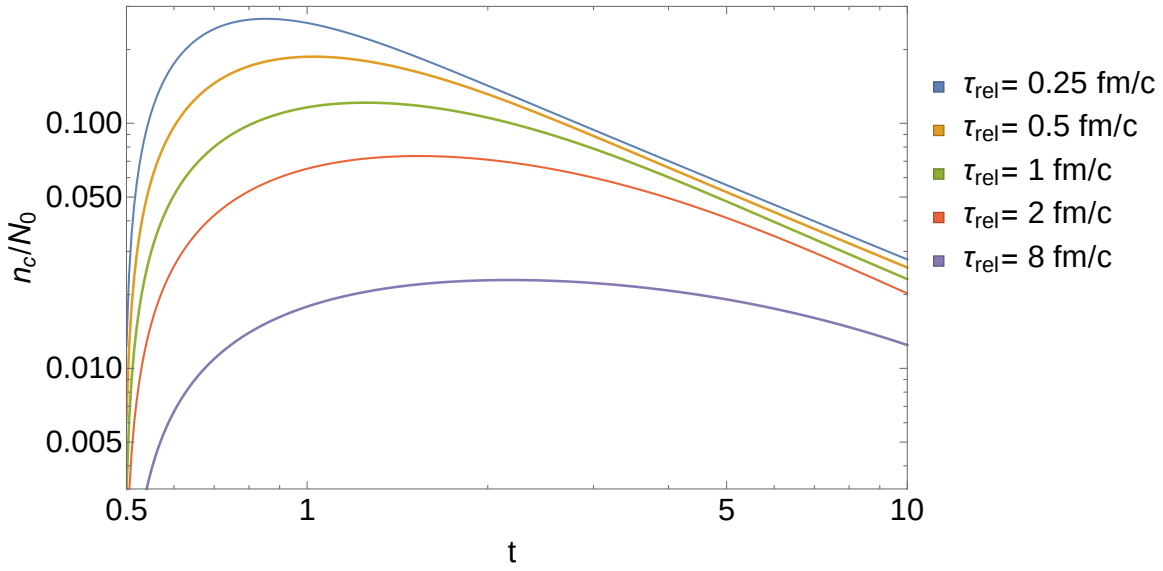

Figure 2.6: Time evolution of the condensate density n_c for several values of the relaxation time parameter τ_{rel}. The condensate builds up more quickly and reaches a larger maximum for smaller τ_{rel}.

In Figure 2.6 we see that the condensate density peaks shortly after the evolution begins, before depleting as the particle content flows out the central slice $z = 0$. For smaller relaxation times, the condensate density remains larger over the course of the evolution shown here.

Chapter 3

Numerics

3.1 Overview

In order to proceed numerically, the distribution function $f(\mathbf{x}, \mathbf{p}, t)$ must be discretized. It is stored as a 3+3+1 dimensional array where each value corresponds to a representative value of the distribution function at a particular spatial and momentum point at a certain time.

Appropriate algorithms to solve the Boltzmann equation must be implemented which maintain positivity of the distribution function, and ensure that numerical artifacts, such as oscillations in the solution are controllable.

The Boltzmann equation describes a complicated "redistribution" of particles throughout six-dimensional phase space which is non-local in character, even in the relaxation time approximation (2.32). To proceed, we opt for a splitting strategy detailed in Section 3.3 which lets us handle the redistribution of particles in physical space and momentum space separately. Such a splitting technique exposes a large portion the parallel character of the problem, which we can exploit with GPU programming.

The Boltzmann equation (2.32) is split into two steps related to the convection and collision terms, $p^\alpha \partial_\alpha f$ and $C_{[f]}$ in (2.32):

1. In the convection step to be outlined in Section 3.4, cells use information from their neighbours in space to compute particle fluxes which transport the particles

throughout space at a constant speed $\mathbf{v} = \mathbf{p}/|\mathbf{p}|$. This procedure is performed individually for each momentum cell.

2. In the collision (relaxation) step detailed in Section 3.5, integrals over all momentum space must be performed at each spatial site in order to calculate the local equilibrium parameters needed for the RTA collision operator. We then evolve the distribution function according to the finite-time relaxation to be defined in (3.17). An appropriate choice of momenta to store the distribution at is crucial in order to maximize accuracy and minimize the number of grid points.

3.2 Tools & Libraries

The code in this project was largely developed in C++ 11. The necessary parallel algorithms were built for use with NVidia CUDA [19] and run on an NVidia GTX 680 GPU. The GNU Scientific Library (GSL) [1] was used for writing the required multi-dimensional root-finding algorithms. Plots were generated and many other calculations were performed in Mathematica 10.

3.3 Splitting Techniques

The Boltzmann equation (2.32) in 3+1 Dimensions involves a complicated evolution over six-dimensional phase space which proves to be numerically challenging [18]. The contributions of the convection and collision term must be treated very differently. This motivates us to attempt to solve each part separately by the so-called "operator splitting" approach and combine the resulting solutions in some clever fashion to approximate the full solution.

The operator splitting assertion begins by assuming that we have the following ODE to solve [18]

$$\frac{d}{dt}f(t) = (\hat{S} + \hat{C})f(t), \tag{3.1}$$

where $\hat{S}$ and $\hat{C}$ are certain linear operators that act on $f(t)$. The formal solution to (3.1) is

$$f(t) = f_0 e^{(\hat{S}+\hat{C})t}, \tag{3.2}$$

where $f_0 = f(t=0)$ is the initial condition.

Let us use a fixed time-stepping procedure such that t^n is the n-th step and $t^{n+1} - t^n = \Delta t$ is the small time step. Then, in order to advance the system in time we have approximately, for $\Delta t \to 0$,

$$f(t^{n+1}) = e^{(\hat{S}+\hat{C})\Delta t} f(t^n). \tag{3.3}$$

Our goal in this procedure is to find a suitable means of using the individual solutions

$$f_1(t^{n+1}) = e^{\hat{S}\Delta t} f_1(t^n), \tag{3.4}$$

$$f_2(t^{n+1}) = e^{\hat{C}\Delta t} f_2(t^n), \tag{3.5}$$

in order to reconstruct the full "solution" (3.3).

Method	Solution operator	Truncation error
Lie Splitting	$e^{\Delta t\hat{S}} e^{\Delta t\hat{C}}$	$\frac{\Delta t^2}{2}[\hat{S},\hat{C}]f(t) + O(\Delta t^3)$
Strang Splitting	$e^{\frac{\Delta t}{2}\hat{S}} e^{\Delta t\hat{C}} e^{\frac{\Delta t}{2}\hat{S}}$	$\Delta t^3(\frac{1}{12}[\hat{C},[\hat{C},\hat{S}]] - \frac{1}{24}[\hat{S},[\hat{S},\hat{C}]])f(t) + O(\Delta t^4)$

Table 3.1: Local truncation errors for different splitting strategies. Higher order terms in the truncation error are similarly comprised of combinations of commutators.

Two of the most common choices of splitting strategies are shown in Table 3.1, which approximate the solution operator in (3.3) with different orders of accuracy, $O(\Delta t^2)$ vs $O(\Delta t^3)$, respectively. In the case that the operators commute, $[\hat{S},\hat{C}] = 0$, splitting schemes become exact.

With the identification of the two operators $\hat{S}f = -\mathbf{v}\cdot\nabla f$ and $\hat{C}f = C_{[f]}$ as the convection term and the collision term respectively, the stepping procedure we use for the Boltzmann equation (2.32) may be stated as

$$f(t^{n+1}) = A_S^{\Delta t/2} A_C^{\Delta t} A_S^{\Delta t/2} f(t^n), \tag{3.6}$$

where we have employed the Strang Splitting, and introduced the stepping operator notation $A_X^{\Delta t} = e^{\Delta t \hat{X}}$. Note that the splitting approaches can be applied [18] to non-linear operators such as $\mathcal{C}_{[f]}$.

We detail the individual approaches to deal with the convection and collision term in the following sections.

3.4 Convection Term

In the limit of no collisions, where $\tau_{rel} \to \infty$, the Boltzmann equation (2.32) becomes

$$\partial_t f(\mathbf{x}, \mathbf{p}) + \mathbf{v_p} \cdot \nabla f(\mathbf{x}, \mathbf{p}) = 0, \tag{3.7}$$

where $\mathbf{v_p} = \frac{\mathbf{p}}{|\mathbf{p}|}$ is the velocity at which particles with four-momentum $p^\alpha = (p_0, \mathbf{p})$ propagate. This is a simple advection equation with solution $f(t, \mathbf{x}) = f_0(\mathbf{x} - \mathbf{v_p} t)$ for a given $\mathbf{p}$ where $f_0(\mathbf{x})$ is the distribution at $t = 0$. Since the streaming velocity $\mathbf{v_p}$ is $\mathbf{p}$-dependent, different $\mathbf{p}$-cells can "mix". Note that whilst this analytic solution is trivial, numerically it poses some challenge to control the numerical artifacts.

The full 3-Dimensional advection equation (3.7) can also be solved via a splitting strategy as outlined in the previous section. Here, we can split the advection into separate 1-Dimensional advections in x, y and z dimensions. This is advantageous since we need only find a suitable one-dimensional algorithm – which is typically simpler – in order to build up the full solution.

If we rewrite (3.7) in terms of operators defined in Section 3.3 we get

$$\begin{aligned} \partial_t f &= \hat{S} f \\ &= -v_x \partial_x f - v_y \partial_y f - v_z \partial_z f \\ &= (\hat{S}_x + \hat{S}_y + \hat{S}_z) f, \end{aligned} \tag{3.8}$$

where we have defined the 1-Dimensional advection operators $\hat{S}_i = -v_i \partial_i$.

To evaluate the truncation error involved in splitting the solution in this way, we look at

how these $\hat{S}_i$ operators commute,

$$\begin{aligned}[\hat{S}_i, \hat{S}_j] &= \hat{S}_i\hat{S}_j - \hat{S}_j\hat{S}_i \\ &= v_i v_j \partial_i\partial_j - v_j v_i \partial_j\partial_i \\ &= 0. \end{aligned} \tag{3.9}$$

Since the operators commute, according to Table 3.1 all splittings are exact, and so we can employ a splitting technique to solve full the 3-Dimensional advection equation by separate 1-Dimensional advections without introducing any additional error beyond 1-Dimensional discretization errors. Then Lie splitting in Table 3.1 is the simplest choice:

$$f(t^{n+1}) = A_{S_x}^{\Delta t} A_{S_y}^{\Delta t} A_{S_z}^{\Delta t} f(t^n). \tag{3.10}$$

3.4.1 Finite Volume Method

The "finite volume method" is a method for numerically solving certain partial differential equations. In particular equations describing hyperbolic conservation laws such as the advection equation (3.7) [17]. This serves as the basis for our 1-Dimensional advection scheme.

Let us introduce a finite set of grid points $(x_{i+1/2})_{i\in I}$ which spans the computational domain $[x_{min}, x_{max}]$. We define a 1-Dimensional spatial cell as $C_i = [x_{i+1/2}, x_{i-1/2}]$ with a width $\Delta x = x_{i+1/2} - x_{i-1/2}$. Given some continuous function $f(t^n, x)$, we take as our new discrete degrees of freedom, the volume average over a cell at time t^n

$$f_i^n = \frac{1}{\Delta x}\int_{x_{i-1/2}}^{x_{i+1/2}} dx f(t^n, x). \tag{3.11}$$

Substitution of the solution to the one-dimensional form of (3.7) into (3.11) lets us observe the effect of averaging the solution over a spatial cell in one time step $t^n \to t^{n+1}$:

$$\begin{aligned}\frac{1}{\Delta x}\int_{x_{i-1/2}}^{x_{i+1/2}} dx f(t^{n+1}, x) &= \frac{1}{\Delta x}\int_{x_{i-1/2}}^{x_{i+1/2}} dx f(t^n, x - v\Delta t), \\ &= \frac{1}{\Delta x}\int_{x_{i-1/2}-v\Delta t}^{x_{i+1/2}-v\Delta t} dx f(t^n, x), \end{aligned} \tag{3.12}$$

where we have used the variable transformation $x \to x + v\Delta t$.

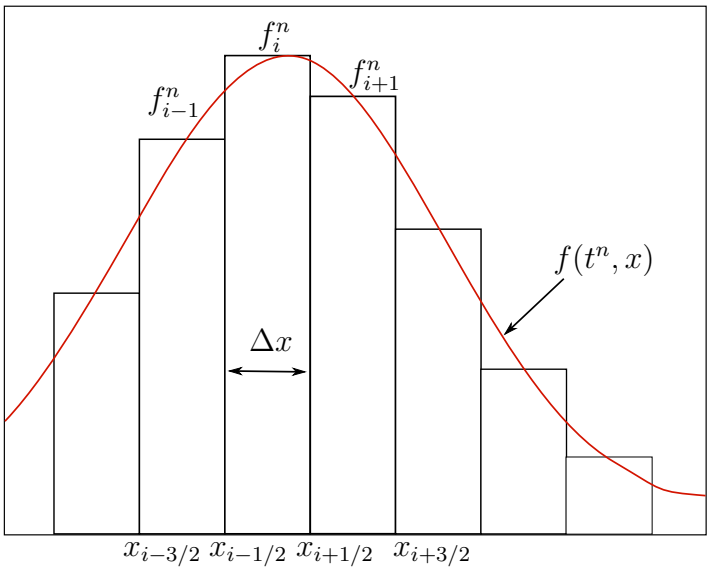

Figure 3.1: Diagram of the volume averages f_i^n illustrating the discretization of some function $f(t^n, x)$.

We further define the flux term

$$\phi_{i+1/2}^n = \frac{1}{\Delta x} \int_{x_{i+1/2}-v\Delta t}^{x_{i+1/2}} dx f(t^n, x). \tag{3.13}$$

If we take f_i^n to represent the distribution function, $\phi_{i+1/2}^n$ is the flux of particles through the cell interface $x_{i+1/2}$, in a time interval Δt.

Making use of (3.12) together with (3.13), we can then write the solution to (3.7) in our discrete formulation as [18]

$$\begin{aligned} f_i^{n+1} &= \frac{1}{\Delta x} \int_{x_{i-1/2}-v\Delta t}^{x_{i+1/2}-v\Delta t} dx f(t^n, x) \\ &= f_i^n + \frac{1}{\Delta x} \int_{x_{i+1/2}-v\Delta t}^{x_{i+1/2}} dx f(t^n, x) + \frac{1}{\Delta x} \int_{x_{i-1/2}-v\Delta t}^{x_{i-1/2}} dx f(t^n, x) \\ &= f_i^n + \phi_{i-1/2}^n - \phi_{i+1/2}^n. \end{aligned} \tag{3.14}$$

This scheme is strictly conservative as the incoming flux of any given cell is equivalent to the outgoing flux of an adjacent cell. It is important to note that through the cell averaging process (3.11), we have not yet introduced any numerics, therefore (3.14) is still exact. However, when we replace the full function with our discrete degrees of freedom (3.11), we lose some details of the continuous function that lets us compute the cell averages and fluxes in the first place. In order to proceed, we must find a suitable means of numerically reconstructing the original function $f(t^n, x)$ from the discrete formulation (3.11). This in turn should let us compute the updated cell averages in a more accurate manner whilst

also satisfying the criteria of particle conservation and semi-positive definiteness, which we expect the original distribution to satisfy.

3.4.2 Positive and Flux conservative method

The Positive and Flux Conservative (PFC) method is a high order reconstruction or interpolation technique that controls spurious oscillations and ensures positivity of the reconstructed function [9, 18]. The authors of [9] derive for a third-order reconstruction,

$$f_h(x) = f_i + \frac{\epsilon_i^+}{6\Delta x^2}[2(x-x_i)(x-x_{i-3/2}) + (x-x_{i-1/2})(x-x_{i+1/2})](f_{i+1}-f_i) \\ - \frac{\epsilon_i^-}{6\Delta x^2}[2(x-x_i)(x-x_{i+3/2}) + (x-x_{i-1/2})(x-x_{i+1/2})](f_i - f_{i-1}), \tag{3.15}$$

for $f = f(t^n, x)$ over cell $C_i = [x_{i-1/2}, x_{i+1/2}]$, using the fixed stencil[1] $\{x_{i-3/2}, x_{i-1/2}, x_{i+1/2}, x_{i+3/2}\}$.

In (3.15) nonlinear slope correctors ϵ_j^+ and ϵ_j^- are introduced in order to ensure positivity $f_i \geq 0$,

$$\epsilon_i^+ = \begin{cases} \min(1; 2f_i/(f_{i+1}-f_i)), & \text{for } f_{i+1}-f_i > 0. \\ \min(1; -2(f_\infty - f_i)/(f_{i+1}-f_i)), & \text{for } f_{i+1}-f_i < 0. \end{cases},$$

$$\epsilon_i^- = \begin{cases} \min(1; 2(f_\infty - f_i)/(f_i - f_{i-1})), & \text{for } f_i - f_{i-1} > 0. \\ \min(1; -2f_i/(f_i - f_{i-1})), & \text{for } f_i - f_{i-1} < 0. \end{cases},$$

where $f_\infty = \max_{j\in I}\{f_j\}$. We assume that outside the boundaries of our computational grid, the distribution is vanishing: $\forall i \notin I,\ f_i^n = 0$.

It can be shown [9] that the above reconstruction satisfies two essential requirements:

Conservation of the average: $\forall i \in I,\ \int_{x_{i+1/2}}^{x_{i+1/2}} dx f_h(x, t^n) = \Delta x f_i^n$.

The maximum principle: $\forall x \in (x_{\min}, x_{\max}),\ 0 \leq f_h(x, t^n) \leq f_\infty$.

[1] The stencil defines the set of surrounding cells which are used to compute the function reconstruction for cell C_i. The stencil is fixed in the sense that this dependence will remain the same, whereas a dynamic stencil allows this to change – typically it will be resized to the version which provides the smoothest approximation to the reconstructed function. Higher order reconstructions require larger stencils as they need to numerically define higher order derivatives in terms of finite differences [9].

With this function reconstruction, we can directly compute the fluxes $\phi_{i+1/2}$ in (3.14) and update our discrete representation of the distribution function (3.11).

An advantage of a scheme based on a fixed stencil such as used in (3.15), is that it is better suited to a parallel implementation. The value of f_i^{n+1} depends only upon $\{f_{i-1}^n, f_i^n, f_{i+1}^n\}$ - namely its value at the previous time step as well as those of its immediate neighbours. Performing this update on a large grid thus involves many similar operations that are largely independent of each other, enabling simultaneous parallel calculation.

3.5 Collision Term - Relaxation

In a homogeneous region of space – as is the case in the splitting solution (3.5) – the Boltzmann equation (2.32) is

$$\partial_t f(\mathbf{x}, \mathbf{p}) = \frac{p^\alpha u_\alpha}{p_0} \frac{f_\infty(\mathbf{x}, \mathbf{p}) - f(\mathbf{x}, \mathbf{p})}{\tau_{rel}}, \tag{3.16}$$

which describes a spatially homogeneous system with flow velocity $\mathbf{u}$. The solution outlined in subsection 3.5.1 in a single time update is to first order

$$f(t + \Delta t) = f(t) + \frac{\Delta t}{\tau_k}(f_\infty(t) - f(t)), \tag{3.17}$$

where we have defined a "boosted" relaxation time

$$\tau_k = \frac{p_0}{p^\alpha u_\alpha} \tau_{rel}. \tag{3.18}$$

Note that written in this way, the solution is consistent with the conservation laws, but may not ensure positivity of the distribution function. Namely if in (3.16), for some momenta $\mathbf{p}$, $f(t) > f_\infty(t)$, the second term will dominate $f(t)$ unless Δt is sufficiently small.

The equilibrium parameters for $f_\infty \equiv f_\infty(T, \mu)$ are found according to (2.39). We have a discrete formulation of the distribution function, so whilst we don't store the full continuum of momenta, our discrete representation allows us to calculate the required moments of f with sufficient accuracy. We detail this in Appendix C.

3.5.1 Finite time relaxation

The finite-time "solution" to (2.32) for a system in a homogeneous box with a finite flow $\mathbf{u}$ is

$$f(t+\Delta t) = f_\infty(t) + (f(t) - f_\infty(t))e^{-\frac{\Delta t}{\tau_k}}, \tag{3.19}$$

for an equilibrium f_∞ which remains constant in time (See our discussion on the running equilibrium in Section 2.6).

Since we are neglecting convective effects, we require that this solution satisfies the energy conservation law $\dot{T^{0\beta}} = 0$ and optionally also $\dot{J^0} = 0$ when we also conserve particle number.

Let's consider the Taylor expansion of (3.19) for small time step Δt

$$\begin{aligned} f(t+\Delta t) &= f_\infty + (f(t) - f_\infty)\exp(-\frac{\Delta t}{\tau_k}) \\ &= f_\infty + (f(t) - f_\infty)\sum_{n=0}^{\infty}\frac{(-1)^n}{n!}\left(\frac{\Delta t}{\tau}\right)^n\left(\frac{p^\alpha u_\alpha}{p_0}\right)^n \\ &= f_\infty + (f(t) - f_\infty)(1 - \frac{\Delta t}{\tau_k} + \ldots) \\ &\simeq f_\infty + f(t) - f_\infty - \frac{\Delta t}{\tau_k}(f_\infty - f(t)) \\ &\simeq f(t) + \frac{\Delta t}{\tau_k}(f_\infty - f(t)). \end{aligned} \tag{3.20}$$

We can check the conservation laws by integrating the approximate solution (3.20) over all momenta

$$T^{\alpha\beta}_{[f]}(t+\Delta t) \simeq T^{\alpha\beta}_{[f]}(t) + \Delta t\int dP p^\alpha p^\beta \frac{(f_\infty - f(t))}{\tau_k} \simeq T^{\alpha\beta}_{[f]}(t) + \frac{\Delta t}{\tau}\int dP p^\alpha p^\beta \frac{p^\gamma u_\gamma}{p_0}(f_\infty - f(t)).$$

For $\alpha = 0$, we find for the temporal components of the energy momentum tensor

$$\begin{aligned} T^{0\beta}_{[f]}(t+\Delta t) &\simeq T^{0\beta}_{[f]}(t) + \frac{\Delta t}{\tau}\int dP p_0 p^\beta \frac{p^\gamma u_\gamma}{p_0}(f_\infty - f(t)) \\ &\simeq T^{0\beta}_{[f]}(t) + \frac{\Delta t}{\tau}u_\gamma\int dP p^\beta p^\gamma (f_\infty - f(t)) \\ &\simeq T^{0\beta}_{[f]}(t) + \frac{\Delta t}{\tau}u_\gamma(T^{\gamma\beta}_\infty - T^{\gamma\beta}_{[f]}) \\ &\simeq T^{0\beta}_{[f]}(t). \end{aligned} \tag{3.21}$$

where in the last step we have used the conservation laws (2.39) for energy and momentum. In words, to 1st order in Δt, the temporal components of the EM tensor $T^{0\beta}$ are conserved.

If we consider the second order term of $T^{0\beta}(t+\Delta t)$,

$$\begin{aligned}&\frac{\Delta t^2}{\tau^2}\int dP p_0 p^\beta \left(\frac{p^\delta u_\delta}{p_0}\right)\left(\frac{p^\gamma u_\gamma}{p_0}\right)(f_\infty - f(t))\\ &= \frac{\Delta t^2}{\tau^2} u_\gamma u_\delta \int dP p_0 p^\beta \frac{p^\gamma}{p_0}\frac{p^\delta}{p_0}(f_\infty - f(t)),\end{aligned} \tag{3.22}$$

we can see that this does not automatically vanish by the conservation laws, except for $\beta = 0$,

$$\begin{aligned}&\frac{\Delta t^2}{\tau^2} u_\gamma u_\delta \int dP p_0 p_0 \frac{p^\gamma}{p_0}\frac{p^\delta}{p_0}(f_\infty - f(t))\\ &= \frac{\Delta t^2}{\tau^2} u_\gamma u_\delta \int dP p^\gamma p^\delta (f_\infty - f(t))\\ &= \frac{\Delta t^2}{\tau^2} u_\gamma u_\delta (T^{\gamma\delta}_\infty - T^{\gamma\delta}_{[f]})\\ &= 0.\end{aligned} \tag{3.23}$$

For the particle current, through the Taylor expansion of (3.19) we find

$$\begin{aligned}J^\alpha_{[f]}(t+\Delta t) &\approx J^\alpha_{[f]}(t) + \Delta t \int dP p^\alpha \frac{(f_\infty - f(t))}{\tau_k}\\ &= J^\alpha_{[f]}(t) + \frac{\Delta t}{\tau}\int dP p^\alpha \frac{p^\gamma u_\gamma}{p_0}(f_\infty - f(t)),\end{aligned} \tag{3.24}$$

The temporal component $\alpha = 0$ is

$$\begin{aligned}J^0_{[f]}(t+\Delta t) &\simeq J^0_{[f]}(t) + \frac{\Delta t}{\tau}\int dP p_0 \frac{p^\gamma u_\gamma}{p_0}(f_\infty - f(t))\\ &\simeq J^0_{[f]}(t) + \frac{\Delta t}{\tau} u_\gamma \int dP p^\gamma (f_\infty - f(t))\\ &\simeq J^0_{[f]}(t) + \frac{\Delta t}{\tau} u_\gamma (J^\gamma_\infty - J^\gamma_{[f]}),\end{aligned} \tag{3.25}$$

which may or not be conserved to 1st order in Δt, depending on whether we include particle conservation or not. If we do, the second term in (3.25) vanishes.

We find that higher order contributions to these expansions in Δt do not vanish in general, and therefore may lead to the violation of the conservation laws at $O(\Delta t)$ for energy,

momentum and particle number (when we choose to conserve it). This motivates the use of the first order approximation (3.16) over (3.19), as we can strictly enforce energy and momentum conservation, and can choose whether or not to also describe particle conservation.

The spatial components of T^{ij} and J^i are free to change, and will do so to become consistent with an equilibrium form at late times.

Chapter 4

3+1 Pilot Study

4.1 Initial Conditions

The results given here are for initial conditions merely inspired by heavy ion collisions. A good opportunity for future work is to consider more interesting and physical distributions, but present results suffice as a proof of concept to demonstrate the validity of the code.

For the time being, we consider as our "nucleus" a uniformly dense sphere of thermalized gluon matter. The distribution function representing each of these "nuclei" is then

$$f_N(\mathbf{x}, \mathbf{p}) = \left(\frac{1}{e^{|\mathbf{p}|/T} - 1} \right) \Theta(1 - |\mathbf{x}|/R), \tag{4.1}$$

where Θ is the Heaviside function and R is representative of the nuclear radius. The initial temperature T is assumed to be uniform over the volume of each nuclei. In a typical heavy ion collision, the nuclei are accelerated to approximately $u \approx 0.99995$ c and so are Lorentz contracted along the beam axis by $\gamma \approx 100$ [14]. We therefore boost each distribution to near-to-light speed through a Lorentz boost $f(x, p) \to f(x', p')$ to represent this. We may furthermore specify an impact parameter b to model non-central collisions.

Despite this initial (local) equilibrium situation, the strong flow of the medium throughout 3D space will drive the system out of this local equilibrium, unless interactions are sufficiently strong so as to maintain a local equilibrium (as in the ideal hydrodynamic limit $\tau_{rel} \to 0$).

For all the results shown, we choose $R = 8$ fm (typical radius for a gold nucleus), and set the initial temperature $T = 500$ MeV. The nuclei are initialized at a small initial z separation of 4 fm at time $t = 0$ fm/c. We choose our initial time to be $t_0 = 2$ fm/c, when the nuclei completely overlap along the beam axis z. The simulations are run until $t = 9$ fm/c. Whilst we would expect certain regions of the gluon matter to fall below the deconfinement temperature before this time, we let the simulations run their course.

We use a spatial grid with 24 cells per dimension, each with a width of $\Delta x = 1$ fm. For the momentum grid, we employ a 16-point Legendre-Gauss quadrature to determine the momentum cells for the positive and negative subspaces, resulting in a total of 32 cells per momentum dimension. The mapping we use is the second entry in Table C.1 where we set the momentum grid scale $\Lambda = 10$ GeV (See Appendix C).

4.2 Results

Figures 4.1 through 4.3 depict contours of constant energy/particle density, where the brighter regions indicate larger densities. The colouring has been scaled such that the brightest region is the maximum initial density for the given quantity.

Figure 4.1, shows a cross-sectional view of the two "nuclei" colliding, which makes visible the internal energy densities. The energy densities shown in Figure 4.1 depict two of the nuclei colliding off-center $b = 0.5R$ from an initial overlap along z at $t_0 = 2$fm/c. The system expands preferentially along the beam axis z and leaves behind a trail of matter, which continues to expand in all directions.

Figures 4.2 and 4.3 are "closeups" of these regions evolving under varying conditions. We see in Figure 4.2 that a large amount of gluons are produced when particle number is not conserved. This results in a much higher particle density in the region where the nuclei initially overlapped.

We look at snapshots at a late time of 8 fm/c in Figure 4.3, for several values of the relaxation time. We see that in the free streaming limit, the nuclei pass through each

other without interacting, whereas for small relaxation times the nuclei become distorted in the overlap region.

Figures 4.4 and 4.5 quantify the total particle production that occurs over the course of the evolution. They indicate that both stronger interactions and more central collisions result in larger gluon numbers.

(a) $t = 2$ fm/c

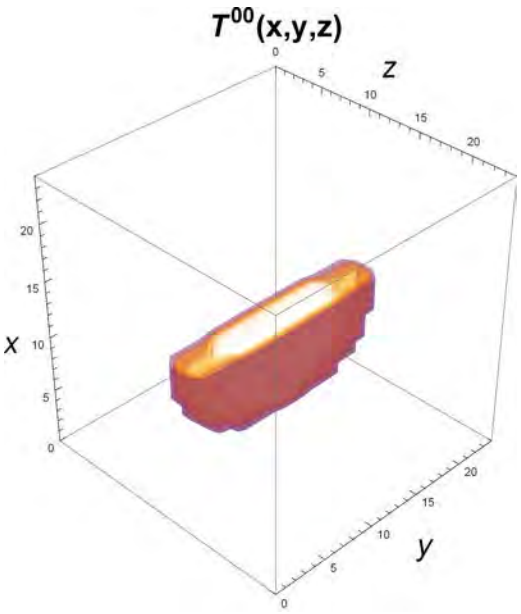

(c) $t = 6$ fm/c

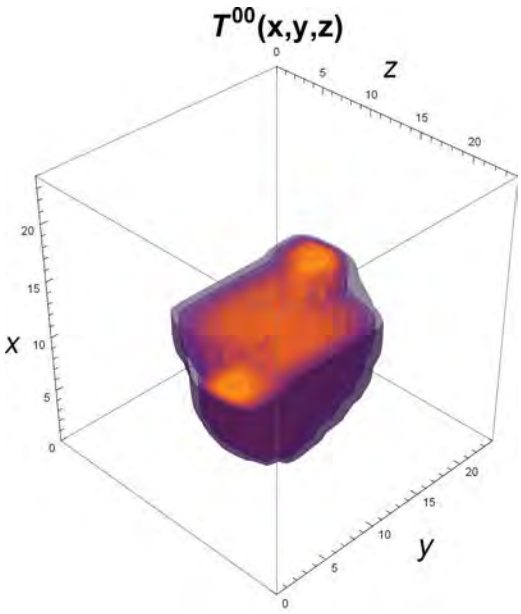

(b) $t = 4$ fm/c

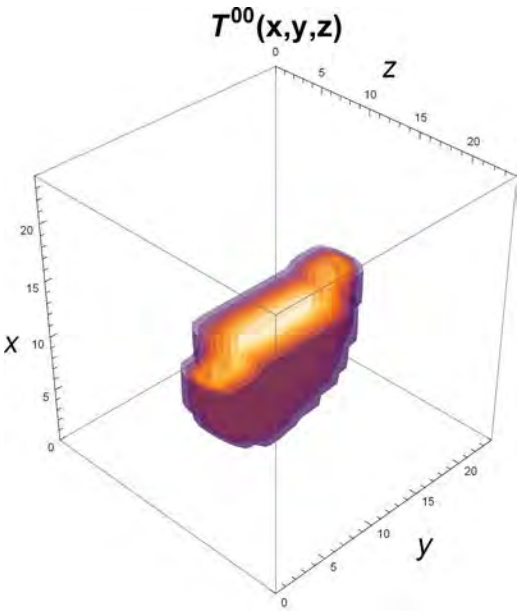

(d) $t = 8$ fm/c

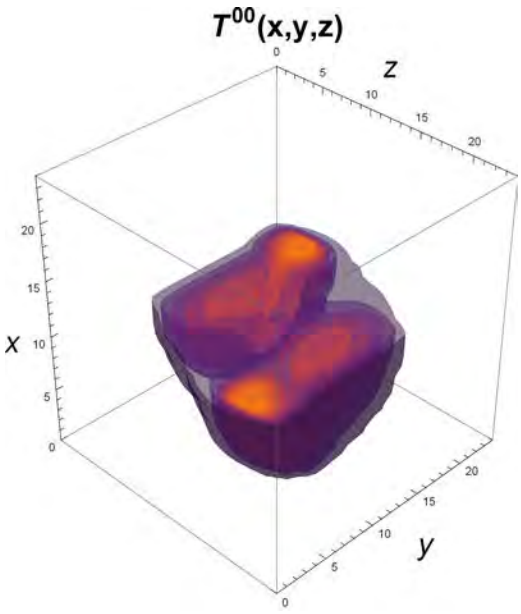

Figure 4.1: Cross-sectional view of the energy density of two colliding gluonic "nuclei" at an impact parameter $b = 0.5R$, with a relaxation time $\tau_{rel} = 2$ fm/c. The figures depict contours of constant energy density, with the brighter regions indicating higher energies.

(a) $J^0(\mathbf{x}, t)$ with particle conservation.

(b) $J^0(\mathbf{x}, t)$ without particle conservation.

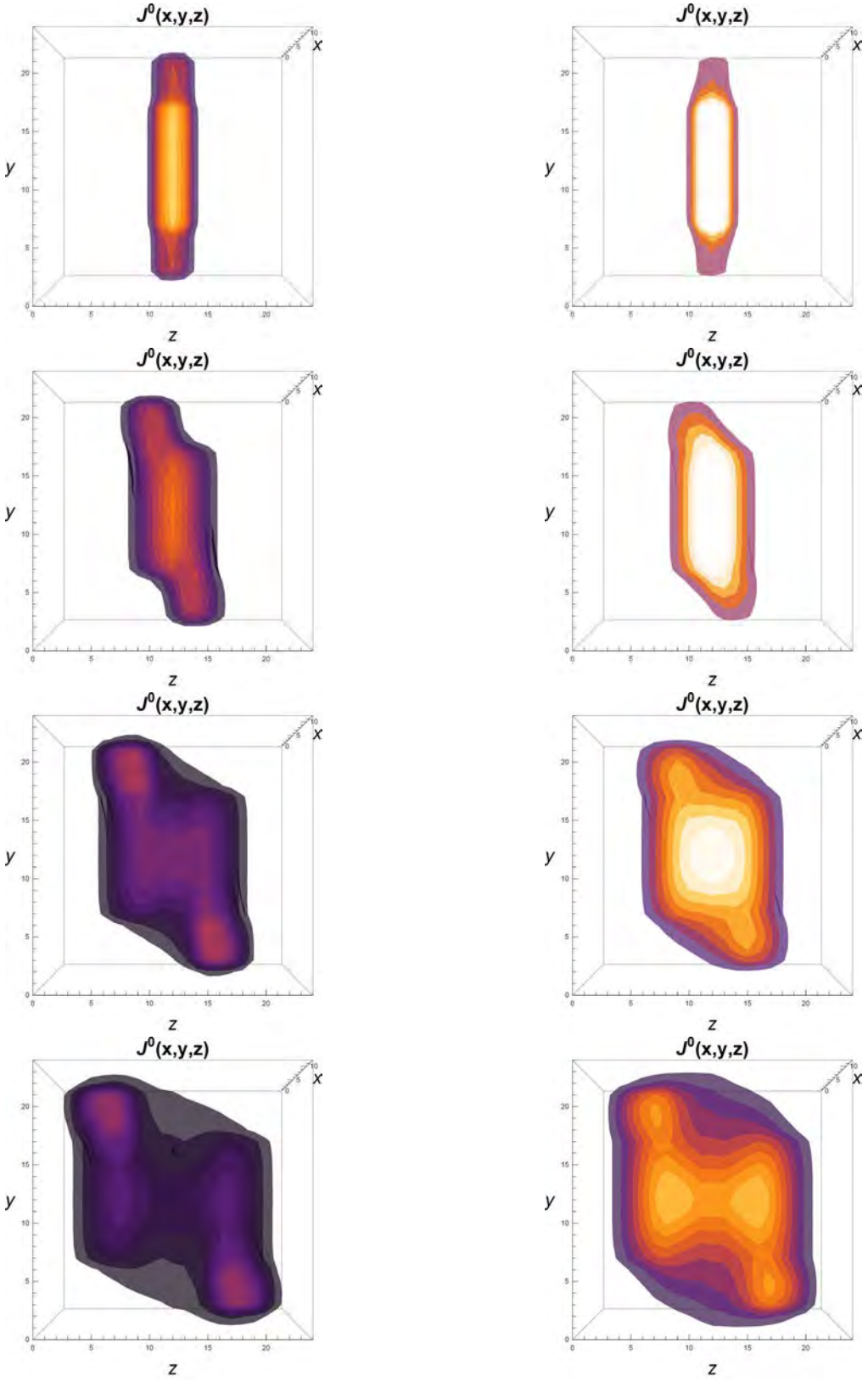

Figure 4.2: Time evolution $t = \{2, 4, 6, 8\}$ fm/c of the particle density $J^0(\mathbf{x})$ in the lab frame for $\tau_{rel} = 2$ fm/c, $b = 0.5$ R , (a) with particle conservation and (b) without particle conservation.

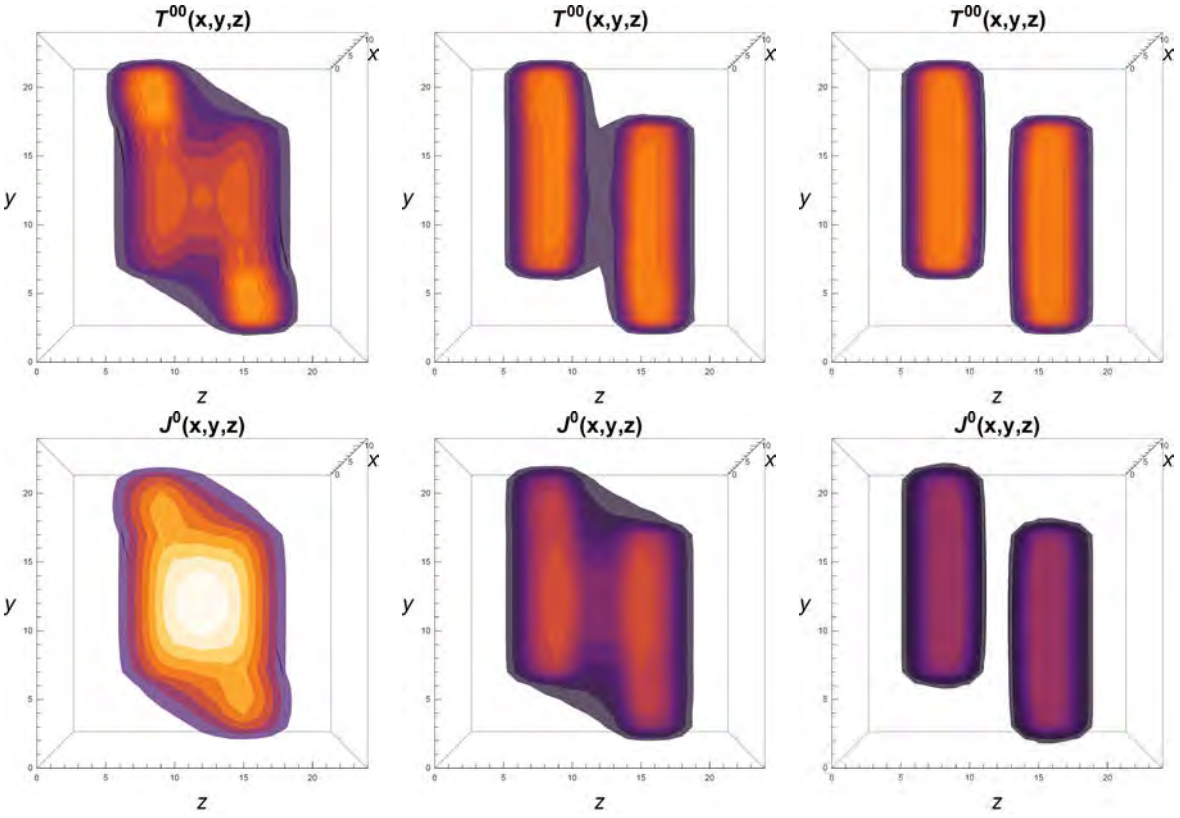

(a) $\tau_{rel} = 2$ fm/c (b) $\tau_{rel} = 16$ fm/c (c) $\tau_{rel} = \infty$

Figure 4.3: Snapshots at time $t = 6$ fm/c of the energy density $T^{00}(\mathbf{x})$ and particle density $J^0(\mathbf{x})$ in the lab frame for three values of the relaxation time τ_{rel}, using impact parameter $b = 0.5R$, neglecting particle conservation. For large relaxation times, the interactions become weaker and the flowing gluon "nuclei" become more transparent.

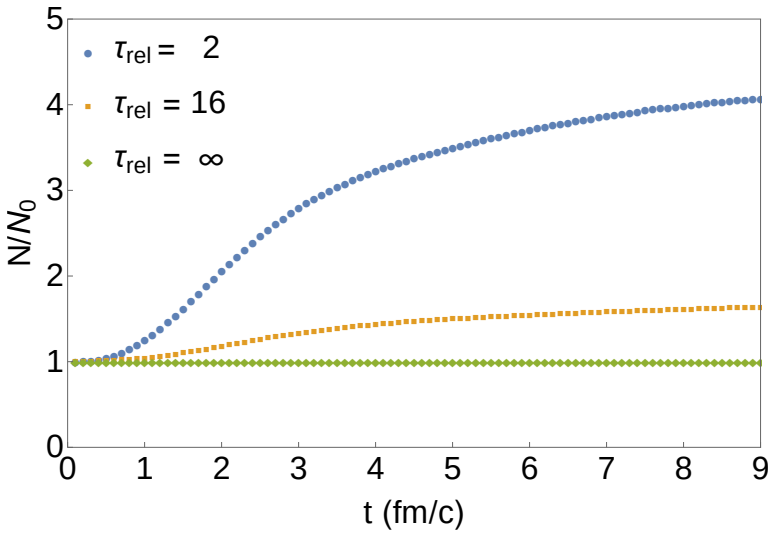

Figure 4.4: The total number of particles in the system $N(t) = \int d^3x J^0(\mathbf{x}, t)$ scaled to the initial value $N(t = 0)$ as a function of time. This was generated according to $\tau_{rel} = \{2, 16, \infty\}$ fm/c, $b = 0.5R$ for an underpopulated initial condition, assuming only energy conservation. This demonstrates that a larger number of particles are produced as the relaxation time is reduced. In the free streaming limit, no particles are produced.

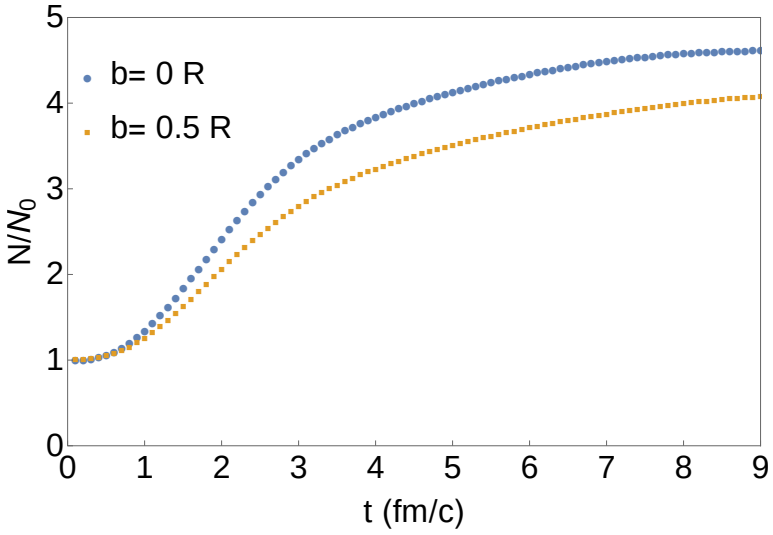

Figure 4.5: The total number of particles in the system $N(t) = \int d^3x J^0(\mathbf{x}, t)$ scaled to the initial value $N(t = 0)$ as a function of time. This was generated according to $\tau_{rel} = 2$ fm/c, $b = \{0, 0.5\}R$ for an underpopulated initial condition, assuming only energy conservation. This demonstrates that for a given relaxation time, reducing the impact parameter b (i.e a more central collision) results in a larger quantity of particles produced.

4.3 Validation of Numerics

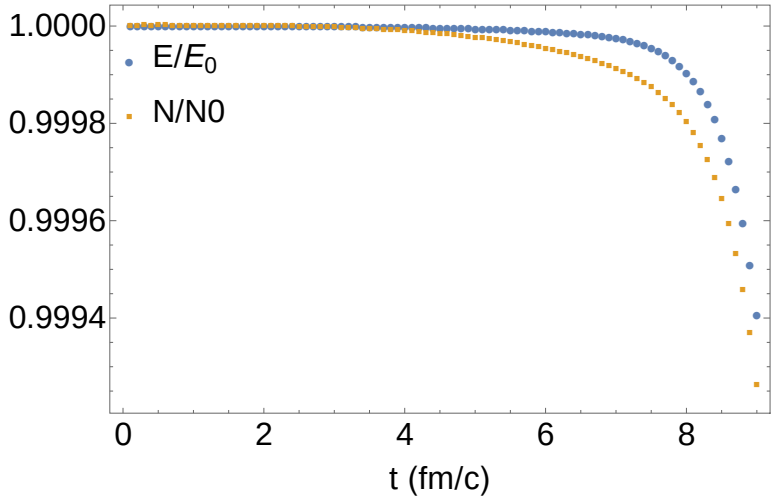

Figure 4.6: Total energy $E(t) = \int d^3x T^{00}(\mathbf{x}, t)$ and total particle number $N(t) = \int d^3x J^0(\mathbf{x}, t)$ of the system scaled to the initial values E_0 and N_0 as a function of time in the free streaming limit $\tau = \infty$ with $b = 0.5R$. This demonstrates that these quantities are conserved numerically within $\approx 0.1\%$. The steep fall-off at about $t \approx 8$ fm/c appears to be related to a certain amount of matter escaping the spatial grid at that point. This demonstrates that our advection algorithm from Section 3 is well behaved, insofar as energy/particle conservation is concerned.

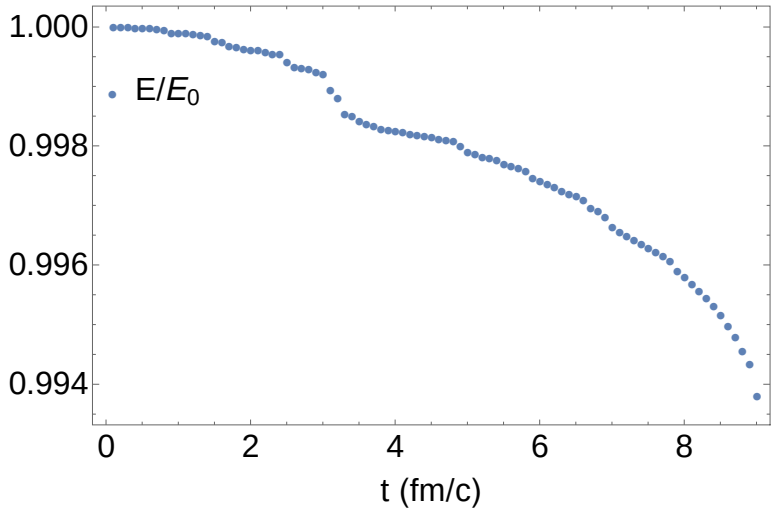

Figure 4.7: The total energy $E(t) = \int d^3x T^{00}(\mathbf{x}, t)$ scaled to the initial value E_0 as a function of time with a finite relaxation time $\tau_{rel} = 16$ fm/c and $b = 0.5R$. The modifications to the distribution function due to collisions reduces the accuracy of the energy conservation to within $\approx 1\%$ over the course of the evolution. Since the shape of the distribution changes due to collisions whilst the momentum grid remains fixed, some loss of accuracy is expected.

Ensuring that the conservation laws hold during the course of the Boltzmann evolution is numerically challenging. This is due to the large number of degrees of freedom of the

full six-dimensional phase space, and the resulting (difficult to predict) evolution of the distribution function.

Figure 4.6 shows the total energy and particle densities in the free streaming limit are well conserved, reducing in value only at late times, when some of the matter begins to exit our spatial grid.

In Figure 4.7 we note that with the addition of interactions, which further modifies the distribution over momentum space, the accuracy is somewhat reduced. Since our numerical momentum grid is static, whereas the distribution function is highly dynamical, some loss of accuracy is expected.

There is a compromise between numerical accuracy and available computational resources, which is especially necessary due to the high dimensionality of our system. Despite this, for a system which we can store on a typical GPU (See section 3.2), we see here that the numerical errors in calculating the overall energy and particle number are actually quite small, remaining within approximately 0.1 - 1% over the course of evolution.

Chapter 5

Summary and Outlook

In this thesis we have developed a parallel implementation to solve the relativistic Boltzmann equation in the relaxation time approximation (2.32) in 3+1 dimensions. We have done so without resorting to simplifying assumptions on the spatial symmetries of the dynamics. This is a significant improvement over existing solvers for the Boltzmann equation, which typically consider only highly symmetric situations [12].

In solving for the distribution function directly, we can gain access to detailed information about the dynamics of a heavy ion collision. This goes beyond the specification of only bulk properties of the medium computable through viscous hydrodynamics [15].

We have showcased in Section (4.2) some first numerical results for a system of interacting gluons undergoing 3 dimensional expansion at ultra-relativistic speeds.

Solving the 3 + 1 Boltzmann equation in a discretized form is a non-trivial task due to numerical artifacts. Therefore we have thoroughly checked that our approach and results are sound with the numerical methods described in Section 3.

We have also shown numerical results for the Boltzmann equation for the case of 0+1 dimensional Bjorken expansion in Section 2.6.1 which we contrasted with existing analytic approximations [3, 5]. This was an initial exploration into the possibility of forming a transient Bose-Einstein condensate.

All of these results are based on the theoretical framework detailed in Section 2 on the relativistic Boltzmann equation in the relaxation time approximation. This approximation is known to capture essential features such as conservation laws and the H-theorem.

The software developed here provides excellent opportunity for future work, as there are many additional features that should be incorporated with regard to application to heavy ion phenomenology. Some possible extensions and investigations include:

- An assumption, which we have employed here, is that the relaxation time is not only momentum independent but also constant in time. However, on physics grounds, τ_{rel} varies with the particle density and transport cross section $\tau_{rel}^{-1} \propto n\sigma_t$ [13], which should be dynamically determined.

- Whilst the code can be easily extended to describe only quarks, in order to describe both gluons and quarks simultaneously, modeling the interactions that exist between them (within the relaxation time approximation) requires further investigation and development.

- As it stands, the equilibrium quantities such as the pressure correspond to that of an ideal (i.e. non-interacting) gas. The incorporation of temperature-dependent effective masses for the gluons will ensure the correct values for these equilibrium quantities [20]. These mass effects also alter the dynamics of the partons, since they will no longer all propagate at light speed. The computational complexity increases due to an additional force term as in (1.1).

- Physical initial conditions based on the CGC/Glasma [14] picture need to be explored more systematically and possible applications of the code to other fields should be explored.

- Below the deconfinement transition, the QGP will hadronize. As such, our Boltzmann implementation could be paired with "freeze-out" codes [25, 15]. This will allow direct comparison of our results with experiment.

- While the relaxation time approximation can be extended in interesting ways, the ultimate long term goal is to include a collision term according to QCD (see (1.2)). This would be an exceptionally challenging task to develop in a full 3+1 scenario.

Appendix A

Definitions

A.1 Riemann Zeta - $\zeta(s)$

$$\zeta(s) = \frac{1}{\Gamma(s)} \int_0^\infty dx \frac{x^{s-1}}{e^x - 1} \tag{A.1}$$

where $\Gamma(s)$ is the gamma function, which for integer s is

$$\Gamma(s) = (s-1)! \tag{A.2}$$

A.2 Polylogarithm - $\mathrm{Li}_s(z)$

The polylogarithm is defined as

$$\mathrm{Li}_s(z) = \sum_{k=1}^{\infty} \frac{z^k}{k^s} \tag{A.3}$$

for any complex s and z, with $|z| \leq 1$.

The polylogarithm is related to an integral over a Bose-Einstein distribution

$$\mathrm{Li}_s(z) = \frac{1}{\Gamma(s)} \int_0^\infty dx \frac{x^{s-1}}{e^x/z - 1}, \tag{A.4}$$

and also an integral over a Fermi-Dirac distribution

$$-\mathrm{Li}_s(-z) = \frac{1}{\Gamma(s)} \int_0^\infty dx \frac{x^{s-1}}{e^x/z + 1}, \tag{A.5}$$

where $z = e^{\mu/T}$ can be identified as the fugacity. For the special case $z = 1$ we have $Li_s(1) = \zeta(s)$.

A.3 Projector Tensor - $\Delta^{\alpha\beta}$

The projector is a rank-2 tensor defined in terms of the fluid velocity u^α [8]

$$\Delta^{\alpha\beta} = g^{\alpha\beta} - u^\alpha u^\beta. \tag{A.6}$$

The contraction of this tensor with an arbitrary four vector, selects out the part transverse to u^α since we have

$$u_\alpha \Delta^{\alpha\beta} = 0. \tag{A.7}$$

The projector satisfies the following properties:

- $\Delta^\alpha_\alpha = 3$,
- $\Delta^{\alpha\beta}\Delta_{\beta\gamma} = \Delta^\alpha_\gamma$,
- $\Delta^\alpha_\beta \Delta^{\beta\gamma} = \Delta^{\alpha\gamma}$.

The projector is also known as the 3-metric, since in the local rest frame where $u^\alpha = (1, \mathbf{0})$, we have $\Delta^\alpha_\beta = \mathrm{diag}(0, 1, 1, 1)$.

Appendix B

Model Properties

B.1 Summational Invariance: $\int dP\psi C_{[f]} = 0$

To prove the first property (2.41), we first substitute the Boltzmann equation (2.32) and make use of the conservation laws (2.39) [8].

For $\psi = a$

$$a \int dP p^\alpha u_\alpha \frac{f_\infty(\mathbf{x},\mathbf{p}) - f(\mathbf{x},\mathbf{p})}{\tau_{rel}} = a(u_\alpha J^\alpha_\infty - u_\alpha J^\alpha_{[f]}) \\ = 0. \tag{B.1}$$

For $\psi = B_\beta p^\beta$

$$B_\beta \int dP p^\alpha p^\beta u_\alpha \frac{f_\infty(\mathbf{x},\mathbf{p}) - f(\mathbf{x},\mathbf{p})}{\tau_{rel}} = B_\beta(u_\alpha T^{\alpha\beta}_\infty - u_\alpha T^{\alpha\beta}_{[f]}) \\ = 0. \tag{B.2}$$

B.2 Boltzmann H-Theorem: $\partial_\alpha S^\alpha \geq 0$

Here we show that the Boltzmann equation (2.32) obeys the second law of thermodynamics (or H-theorem) (2.42) for bosons and fermions [8].

First let us define the differential operator $\mathcal{D} \equiv p^\alpha \partial_\alpha$, and $\bar{f} \equiv 1 + \epsilon f$ where as usual $\epsilon = \{1, -1\}$ for bosons or fermions. We note further that $\mathcal{D}\bar{f} = \epsilon \mathcal{D} f$.

Substitution of the quantum entropy formula (2.23) into the second law (2.22) yields

$$\begin{aligned}\partial_\alpha S^\alpha &= -\partial_\alpha \int dP p^\alpha (f \ln f - \epsilon^{-1} \ln \bar{f} - f \ln \bar{f}) \\ &= -\int dP \mathcal{D} (f \ln f - \epsilon^{-1} \ln \bar{f} - f \ln \bar{f}) \\ &= -\int dP \ln(f/\bar{f}) \mathcal{D} f. \end{aligned} \tag{B.3}$$

Using the summational invariant (2.40)[1], and the property (2.41), we have

$$\int dP p^\alpha u_\alpha (f ln f_\infty / \bar{f}_\infty) = \int dP p^\alpha u_\alpha (f_\infty ln f_\infty / \bar{f}_\infty). \tag{B.4}$$

Substitution of this along with (2.32) into (B.3) give

$$\begin{aligned}\partial_\alpha S^\alpha &= -\int dP \ln f/\bar{f} (p^\alpha u_\alpha \frac{f_\infty - f}{\tau}) - \tau^{-1} \int dP p^\alpha u_\alpha f \ln f_\infty/\bar{f}_\infty + \tau^{-1} \int dP p^\alpha u_\alpha f_\infty \ln f_\infty/\bar{f}_\infty \\ &= u_\alpha \tau^{-1} \int dP p^\alpha (f - f_\infty) \ln \frac{f \bar{f}_\infty}{\bar{f} f_\infty}. \end{aligned} \tag{B.5}$$

For bosons we have $\bar{f} = 1 + f$ and for fermions $\bar{f} = 1 - f$. Recall that for fermions $f < 1$ and $f_\infty < 1$ due to the Pauli-exclusion principle, ensuring a positive argument in the logarithm. Since the factors $\ln \frac{f \bar{f}_\infty}{\bar{f} f_\infty}$ and $(f - f_\infty)$ are simultaneously either positive or negative, the entropy production is strictly non-negative $\partial_\alpha S^\alpha \geq 0$, vanishing only when $f = f_\infty$.

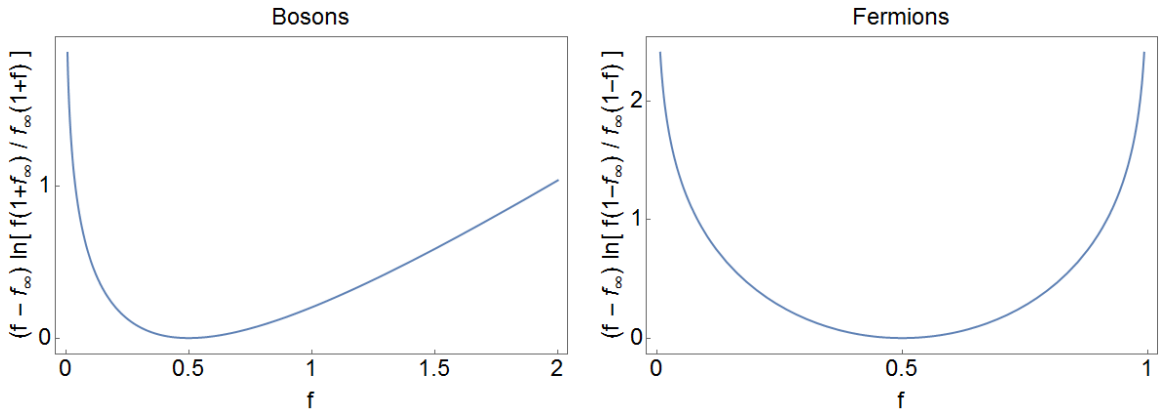

Figure B.1: Plots of $\ln \frac{f \bar{f}_\infty}{\bar{f} f_\infty}$ for increasing f, for bosons and fermions respectively. Here we have chosen $f_\infty = 0.5$, but positivity is ensured for arbitrary values.

[1] If particle number is not conserved, this remains a summational invariant due to a vanishing chemical potential $\mu = 0$.

Appendix C

Gaussian Quadrature

In order to efficiently calculate the various momentum integrals required to find f_∞ in the relaxation step, we must employ accurate numerical integration techniques which let us sufficiently reduce the size of the momentum grid.

The goal of Gaussian quadrature [22] is to find an optimal set of weights w_i and abscissa x_i such that

$$\int_a^b dx W(x) f(x) \approx \sum_{i=1}^{n} w_i f(x_i), \tag{C.1}$$

where $W(x)$ is some weight function and $f(x)$ is the function to be evaluated. Most n-point Gaussian Quadrature are designed to provide exact fits when $f(x)$ is a polynomial of order $(2n-1)$. For our purposes, this means that for sufficiently smooth functions $f(x)$, Gaussian Quadrature will provide high accuracy approximations to the integral (C.1). These methods converge exponentially fast with smooth integrands, because both the order of the method $(2n-1)$, and the density of points increases with n. Uniform grid approaches such as Newton-Cotes on the other hand, have a fixed order for increasing n. Consequently, using Gaussian Quadrature will enable us to approximate the function $f(x)$ by far fewer abscissa than a naive uniform grid discretization. This is of a massive computational advantage to us, especially when we move to higher dimensions.

The weight function $W(x)$ may be chosen in order to exactly cancel an integrable singularity in the function $f(x)$ [22], which may lead to a good approximation to (C.1) if the function is otherwise smooth. Since we expect the distribution function to change greatly

over the course of its evolution, this technique is of little benefit to us. As a result, we employ Legendre-Gauss in our calculations, which for (C.1) corresponds to $W(x) = 1$, $a = -1$, $b = 1$ and the abscissa x_i are the roots of the Legendre Polynomial $P_n(x)$.

In order to calculate integrals over a box of a higher dimension d, the procedure (C.1) is applied to each dimension in turn which yields

$$\int_{-1}^{1} d^d x f(\mathbf{x}) \approx \prod_{j}^{d} (\sum_{i_j}^{n_j} w_{i_j} f(x_{i_j})). \tag{C.2}$$

We finally perform variable transformations in order to map our infinite momentum space to the d-dimensional unit box and numerically compute the macroscopic quantities of interest from the distribution function.

Many Gaussian Quadrature, such as Legendre-Gauss (C.2) are designed to work with functions $f(x)$ defined over a finite interval $x \in (a, b)$. In order to be applicable to our momentum subspace which stretches to infinity, we should choose a suitable variable transformation which maps the compact interval $x \in (a, b)$ to the infinite one, $y \in (-\infty, \infty)$ or semi-infinite one $y \in (0, \infty)$. Here we introduce a momentum scale parameter Λ – see Table C.1 – which ensures correct dimensionality, and lets us scale our final grid to best suit the typical momentum distributions.

y	$J(x) = dy/dx$	$x \in (a, b)$	$y \in (c, d)$
$\Lambda \frac{x}{1-\sqrt{x^2}}$	$\frac{\Lambda}{(\sqrt{x^2}-1)^2}$	$[-1, 1]$	$(-\infty, +\infty)$
$\Lambda(\frac{x}{1-x} + \frac{1}{2})$	$\frac{\Lambda}{(x-1)^2}$	$[-1, 1]$	$(0, +\infty)$
$\Lambda(\frac{x}{(1-x)^2} + \frac{1}{4})$	$-\frac{\Lambda(1+x)}{(x-1)^3}$	$[-1, 1]$	$(0, +\infty)$

Table C.1: Some possible choices of $x \to y$ mappings, and their corresponding Jacobians $J(x)$.

In the case that the mapping in Table C.1 only handles the positive interval, the corresponding negative interval is obtained by simply taking $x \to -x$.

Suppose we wish to approximate the following integral

$$\int_{-\infty}^{\infty} dy f(y). \tag{C.3}$$

We can do so by using a quadrature rule and making the appropriate variable transformation. Our new abscissa will be $\{x_i\}$ and (C.3) becomes

$$\begin{aligned}\int_{-\infty}^{\infty} dy f(y) &= \int_a^b dx J(x) f(y(x))) \\ &= \int_a^b dx g(x) \\ &\approx \sum_{i=1}^{n} w_i g(x_i),\end{aligned} \tag{C.4}$$

where our new integrand is $g(x) = J(x)f(y(x))$.

This procedure readily extends to higher dimensional integrals as

$$\int_{-\infty}^{\infty} d^d y f(y_1, \ldots, y_d) = \int_a^b d^d x \left(\prod_{i=1}^{d} J(x_i) \right) f(y_1(x_1), \ldots, y_d(x_d)). \tag{C.5}$$

Using (C.2) together with (C.5) lets us numerically compute our macroscopic quantities of interest from the distribution function.

Bibliography

[1] Gnu scientific library.

[2] J Anderson. A Relativistic Relaxation-Time Model for the Boltzmann Equation. *Physica*, 74:466–488, 1974.

[3] G Baym. Thermal equilibration in ultra-relativistic heavy-ion collisions. *Phys. Lett. B*, 138(1):18 – 22, 1984.

[4] J D Bjorken. Highly relativistic nucleus-nucleus collision: The central rapidity region. *Phys. Rev. D*, 27:140–151, 1983.

[5] J P Blaizot, F Gelis, J Liao, L McLerran, and R Venugopalan. Bose–einstein condensation and thermalization of the quark gluon plasma. *Nucl. Phys. A*, 873:68–80, 2012.

[6] J P Blaizot and J Liao. Gluon Transport Equations with Condensate in the Small Angle Approximation. *Nucl. Phys. A*, 949:35–47, 2015.

[7] J P Blaizot, J Liao, and L McLerran. Gluon Transport Equation in the Small Angle Approximation and the Onset of Bose-Einstein Condensation. *Nucl. Phys. A*, 920:58–77, 2013.

[8] C Cercignani and G Kremer. *The Relativistic Boltzmann Equation: Theory and Applications*. Birkhäuser Basel, 2002.

[9] F Filbet, E Sonnendrücker, and P Bertrand. Conservative numerical schemes for the vlasov equation. *J. Comput. Phys.*, 172(1):166–187, 2001.

[10] W Florkowski, E Maksymiuk, R Ryblewski, Radoslaw, and M Strickland. Exact Solution of the (0+1)-Dimensional Boltzmann Equation for a Massive Gas. *Phys. Rev. C*, 89(5):054908, 2014.

[11] R Hakim. *Introduction to Relativistic Statistical Mechanics: Classical and Quantum.* World scientific, 2011.

[12] U Heinz, D Bazow, G S Denicol, M Martinez, M Nopoush, J Noronha, R Ryblewski, and M Strickland. Exact Solutions of the Boltzmann Equation and Optimized Hydrodynamic Approaches for Relativistic Heavy-Ion Collisions. In *Proceedings, 7th International Conference on Hard and Electromagnetic Probes of High-Energy Nucleur Collisions (Hard Probes 2015)*, 2015.

[13] A Hosoya and K Kajantie. Transport coefficients of {QCD} matter. *Nucl. Phys. B*, 250(1–4):666 – 688, 1985.

[14] E Iancu. Qcd in heavy ion collisions. In *Proceedings, 2011 European School of High-Energy Physics (ESHEP 2011)*, 2014.

[15] S Jeon and U Heinz. Introduction to Hydrodynamics. *Int. J. Mod. Phys. E*, 24(10):1530010, 2015.

[16] J Kirkwood. The Statistical Mechanical Theory of Transport Processes I. General Theory. *J. Chem. Phys.*, 14:180–201, 1946.

[17] R Luciano and O Zanotti. *Relativistic Hydrodynamics.* Oxford University Press, 2013.

[18] A Narayan and A Klöckner. Deterministic Numerical Schemes for the Boltzmann Equation. *ArXiv e-prints*, 2009.

[19] NVidia. Cuda c programming guide.

[20] A Peshier, B Kampfer, O Pavlenko, and G Soff. A Massive Quasiparticle Model of the SU(3) Gluon Plasma. *Phys. Rev. D*, 54:2399–2402, 1996.

[21] M E Peskin and D V Schroeder. *An Introduction to Quantum Field Theory.* Addison-Wesley, 1995.

[22] W H Press, S A Teukolsky, W T Vetterling, and B P Flannery. *Numerical Recipes 3rd Edition: The Art of Scientific Computing.* Cambridge University Press, 2007.

[23] M Strickland. Anisotropic Hydrodynamics: Three lectures. *Acta Phys. Polon. B*, 45(12):2355–2394, 2014.

[24] D A Teaney. Viscous Hydrodynamics and the Quark Gluon Plasma. *ArXiv e-prints*, 2009.

[25] F Wojciech. *Phenomenology of Ultra-relativistic Heavy-ion Collisions*. World Scientific, 2010.